# Towards Understanding Catalytic Processes for the Reactivity of Hydrocarbons on Rh Surface: A Quantum Chemical Study

DISSERTATION

submitted to the

Faculty of Chemistry and Geosciences
of the Rupertus-Carola University of Heidelberg, Germany
for the degree of
Doctor of Natural Sciences

presented by
Tanushree Bhattacharjee, M.Tech. Chem. Engg.
born in North Tripura, India

Examiner: Prof. Dr. Olaf Deutschmann
Prof. Dr. Uwe Riedel

Heidelberg, 27.06.2011

Interdisciplinary Centre for Scientific Computing
Ruperto-Carola University of Heidelberg

# Towards Understanding Catalytic Processes for the Reactivity of Hydrocarbons on Rh Surface: A Quantum Chemical Study

Examiner: Prof. Dr. Olaf Deutschmann
Prof. Dr. Uwe Riedel

# Abstract

The demand of compact and energy saving procedures for the synthesis of $H_2$, synthesis gas and olefins from hydrocarbon fuel is expanding very rapidly as these are essentially needed in fuel cells, additive for fuel and for the cleaning and purification of flue gas. The concern is in particular to more efficient and environmentally more compatible concepts of the energy supply and reduction of pollutant emissions in mobile and stationary applications. Aliphatic hydrocarbons can be reformed efficiently through catalyst aided partial oxidation over noble metals such as rhodium and the hydrocarbons can also be converted into basic chemical substances. Due to the complex interaction between homogenous and heterogeneous reaction as well as transport processes, many experimental findings could not be interpreted till now. Only with models which are based on molecular processes, it will be possible to understand the catalysis and surface science chemistry better. Computational studies can be very useful in understanding the interaction of adsorbates with metal surfaces. These studies allow obtaining information that is difficult to measure experimentally such as adsorption energies, geometries of adsorbed molecules and activation energy of surface reactions in particular. The aim of the present work is to study the reactions relevant to partial oxidation of $C_1$, $C_2$ and $C_3$ hydrocarbons in catalytic surface of rhodium by first principles calculations. DFT simulation of individual elementary step reactions is carried out. The kinetic parameters and derivative of thermodynamic data is obtained by means of the program CASTEP and VASP, which are based on periodic boundary conditions**.** The detailed comprehension of the surface processes enables to improve understanding of the partial oxidation catalysis occurring at Rh surface.

# Zusammenfassung

Die Nachfrage nach platz- und energiesparenden chemischen Prozessen zur Synthese von Wasserstoff, Synthesegas und Olefinen aus Erdöl nimmt sehr stark zu, da diese Prozesse unverzichtbar sind für Brennstoffzellen, Treibstoffzusätzen sowie zur Reinigung von Abgasen. Das Interesse liegt hier speziell in effizienteren und umweltschonenderen Konzepten für die Energieversorgung und in der Reduktion von Schadstoffemissionen in mobilen und stationären Anwendungen. Alphatische Kohlenwasserstoffe können effizient reformiert werden durch partielle Oxidation katalysiert an Edelmetallen, z.B. Rhodium und die Kohlenwasserstoffe können auch in Basischemikalien umgewandelt werden. Aufgrund des komplexen Zusammenspiels zwischen homogenen und heterogenen Reaktionen als auch mit Transportprozessen konnten viele experimentelle Ergebnisse bis jetzt nicht interpretiert werden. Nur mit Modellen welche auf molekularen Prozessen beruhen wird es möglich sein die Katalyse und Oberflächenchemie besser zu verstehen. Numerische Studien können sehr nützlich sein um die Interaktion zwischen Adsorbaten und Metalloberflächen zu verstehen. Diese Studien erlauben den Zugang zu Information welche experimentell schwer messbar ist, z.B. Adsorbtionsenergien und Geometrien oder Aktivierungsenergien. Das Ziel dieser Arbeit ist die Studie der relevanten Reaktionen bei der partiellen Oxidation von $C_1$, $C_2$ und $C_3$ Kohlenwasserstoffen auf einer katalytischen Rhodiumoberfäche mittels numerischen ab inito Rechnungen. DFT Simulationen von elementaren Reaktionen werden durchgeführt. Die kinetischen Parameter und Ableitungen von thermodynamischen Daten werden mit dem Programm CASTEP und VASP, welche beide mit periodischen Randbedingungen arbeiten, errechnet. Die detaillierte Einsicht in die Oberflächenprozesse erlaubt ein verbessertes Verständnis in die rhodiumoberflächen-katalysierte partielle Oxidation.

# Contents

# Chapter 1

# Introduction

## 1.1 Background

The world's unquenchable necessity for energy has highlighted the demand for a continued supply of inexpensive clean energy that is not only sustainable, but also satisfies regulations for environmental emission issues. Synthesis gas, also referred as syngas, which is a building block in alternative fuels, is one of such indispensable components. With the ever-increasing worldwide demand for synthesis gas, alternative, efficient ways to produce synthesis gas in industry are highly desired. Alkane is a source of economic raw materials, the functionalization of which by selective or partial oxidation [1-4] has attracted considerable interest over decades to produce syngas. Hydrogen, which is the key component of syngas produced, is however a key product and potential fuel of the future as it can be used in fuel cells for stationary and mobile applications and is known to be an energy carrier. It can also be produced from fossil fuels through various processes like reforming using natural gas, naphtha, gasoline, or even heavier fuels like diesel, gasoil, etc. Natural gas, which is mainly methane, is one of the most attractive sources which accounts for almost half the feedstock used for $H_2$ production in the world and has the lowest greenhouse effect in terms of $CO_2$ emissions, in addition to high conversion efficiency and a wide transportation network [5–7]. LPG is also a promising fuel because of similar reasons and also both of its components, propane and butane, have high conversion efficiencies [8–10].

Major technologies used to produce hydrogen from hydrocarbon fuels are steam reforming and catalytic partial oxidation. Steam reforming requires large-scale

converters and in addition is very energy demanding. Catalytic partial oxidation however can be carried out in miniature reactors and is a less energy intensive process. The reaction is thermochemically controlled in which initially, hydrocarbons are fully oxidized to carbon dioxide and water, and the catalyst heats up rapidly owing to the strongly exothermic reactions. With increasing temperature, the system is steered in the direction of the less exothermic pathway, leading to the formation of desired products as CO and hydrogen. Thus, selectivity towards useful partial oxidation compounds can only be accomplished via kinetic control, but that requires a good understanding of the surface reaction mechanisms. First principles quantum mechanical calculations are becoming an indispensable tool in the fields of surface science and heterogeneous catalysis. Qualitative and also quantitative insights into surface chemistries can be efficiently obtained with first principles techniques.

## 1.2 Catalytic Processes on Metal Surfaces

The adsorption of hydrocarbons onto the surfaces of transition metals is a subject of great interest in catalysis due to its importance in many catalytic processes e.g. hydrogenation, dehydrogenation and isomerization. The electronic interaction of molecules with the surface will play a role in the bonding of reactants to the surfaces of the catalyst. The first approach to studying the surface chemistry of hydrocarbons on metal catalysts was obtained by modeling single-crystal surfaces [11, 12]. Although these studies neglect the effect of the support and particle size, they do reveal certain aspects of how surface reactions proceed and can significantly contribute to our understanding of heterogeneous catalytic processes.

### 1.2.1 Development of Experimental Techniques

On the experimental front, there has been tremendous progress towards detecting and understanding the chemistry of species generated by adsorption

over metal catalysts during the past few decades. The preparation and spectroscopic characterization of single-crystal surfaces, exquisite control of the deposition of adsorbates by molecular beam methods, quantum state–specific probing of desorbed species by laser techniques, and the ability to image individual atoms and molecules with the microscopic techniques have gone a long way toward removing the shroud of uncertainty from the field of surface chemistry [13–17]. As a result of the emergence of definitive and quantitative experiments, theoretical treatments of adsorbate-surface interactions have blossomed. Various spectroscopies like NEXAFS, UPS, TDS, TOF-SIMS, RAIRS etc. and other experimental techniques provides information on adsorbed surface species. **Figure 1.1** presents some of these surface science techniques for characterization of adsorbate on a surface and provides the information we can obtain from the corresponding techniques.

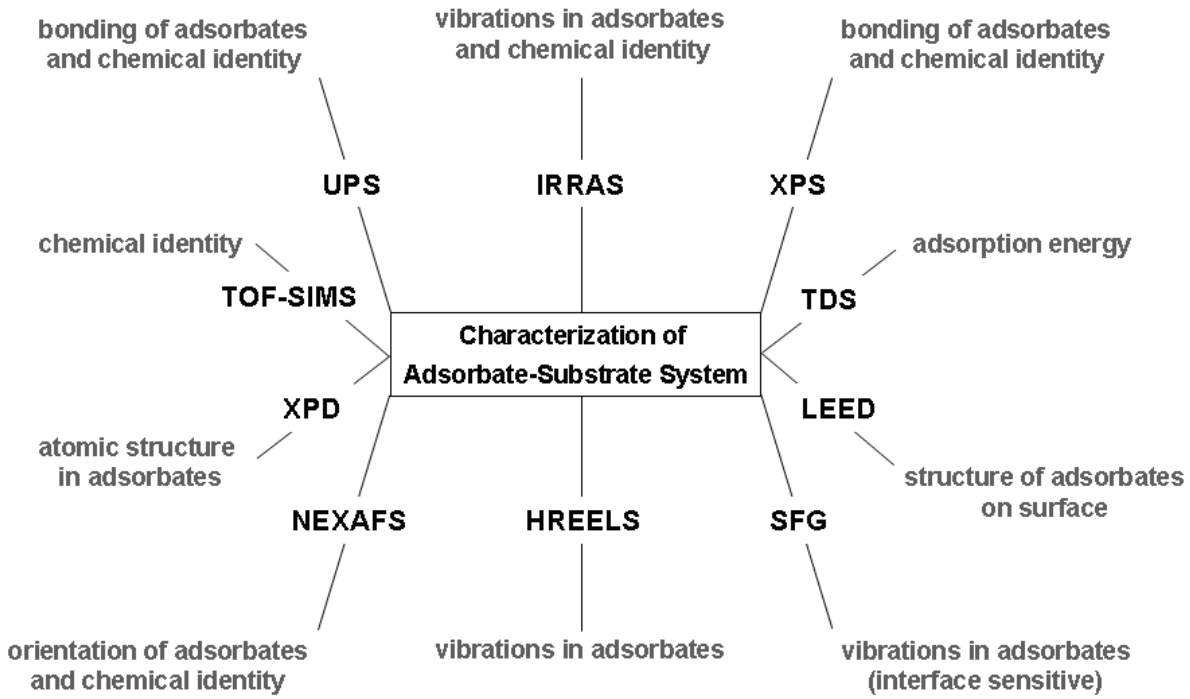


**Figure 1.1** Common experimental techniques for characterization of Adsorbate-surface system

These techniques require very expensive instrumentation, cumbersome procedures and complex mathematical treatments of the data. It is now possible with theoretical calculations to lead a rigorous way to assign all the observed frequencies and no extra cost is required. The geometrical information of the surface species can also obtained with good accuracy.

### 1.2.2 Projection of Theoretical Chemistry Computations

Experimental investigations in surface science and catalysis often raise intriguing questions that cannot be easily answered by the experiments themselves. In such situations, it is sometimes possible to explain the resulting puzzles by attacking the problem with theoretical methodologies. Characterization of active sites and the detection of reaction intermediates by experiments were always very difficult. Moreover, the short-lived transition states are extremely challenging and impossible to study by direct experiment. So, structural elucidation of surface intermediates which have very small concentration and very short lifetime and also taking deeper insights into the otherwise inaccessible reaction pathways are only possible through advances in theoretical modeling. Theoretical chemistry hence starts to be of increasing use for a better understanding of chemical processes at the molecular level. The choice of Semi-empirical, density functional, and ab-initio quantum mechanical methods will however depend on the complexity of the electronic situation in the reactive subsystem and on the desired accuracy of the treatment.

Initially, the empirical methods were used as tools for studying organic and inorganic molecules. The post-HF methods improved the electronic structure scenario and gave very accurate results. Though all these methods have helped to develop the understanding of overall surface processes better yet their applications remain restricted to rather small systems.

The Semi-empirical quantum chemical methods like bond order conservation–Morse potential (BOC-MP) method, Extended Hückel theory, Applications of the

atom superposition and electron delocalization molecular orbital (ASED-MO) method were also developed in time which made many approximations and obtain some parameters from empirical data. The unity bond index—quadratic exponential potential (UBI-QEP) method became popular which is an extension of the BOC-MP method of Shustorovich. This technique models the energetics of reactions on transition metal surfaces and has been employed with considerable success by a number of researchers.

With the development of first principles calculations, which have a number of features that allow them to make important contributions to the investigation of adsorbate-surface interactions. First, the simulations can be performed at almost any degree of spatial resolution, thus making it possible to accurately determine the geometries, energies, electronic structures, and site preferences of adsorbates on well-defined solid surfaces. Besides, the inputs to simulations can be easily controlled, eliminating concerns about the effects of contaminants or other unknown variables.

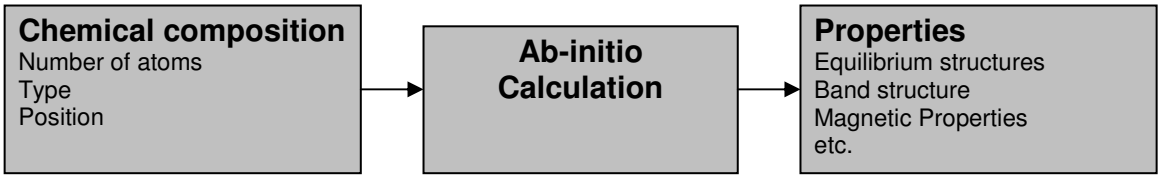


**Scheme 1.2.** Inputs and output of ab-initio calculations

The results ab-initio simulations are generally easier to interpret than are the results of experiments, although wavefunctions and other outputs from theoretical simulations can be quite complex, it is usually possible to create software to analyze these numerical data quickly and efficiently.

The Density Functional Theory (DFT) based methods emerge as an attractive alternative way to study heterogeneous catalytic processes, which became very popular and after the Nobel Prizes awarded to Professors John A. Pople and Walter Kohn in 1990 and put forward a significant milestone in the development

of ab-initio methods. With acceptable computational demands, DFT is nowadays an optimal tool for achieving a good accuracy in calculation results. Thus, theoretical modeling and simulation enables us to understand the existing systems better, complement experimental findings and also provide additional information for continuous new system development in various areas like for catalysis.

## 1.3 Model Catalysts

A good choice for a catalyst can decrease reaction barriers, thereby providing means to selectively convert reactants to the desired products under mild conditions. A catalyst is regenerated during the reaction cycle, leading to its availability to be used again. Metal surfaces are key components in a wide range of technologically important catalyst materials and the reactivity is vital to processes such as sintering, catalysis and corrosion. Transition metals due to their interesting properties are extensively used in catalysis and they are widely studied during the past decades. Nonetheless, the oxidation mechanisms of hydrocarbon molecules on metals are not fully understood. Understanding the whole process at a molecular level is highly desirable for design and optimization of microchemical devices. Platinum, palladium, rhodium and nickel, despite their close structural relationship and their proximity in the periodic table, show several significant differences in their chemistry. It is found that Rh has higher activity and superior selectivity towards synthesis gas formation compared to other transition metals like Pt while Ni and Pd are not found suitable as they lead to sintering and oxygenates formation. The use of Rh directs the conversion of natural gas and oxygen to synthesis gas at contact times of few milliseconds under adiabatic conditions and can be used as a model catalyst to study hydrocarbons for catalytic partial oxidation.

## 1.4 Scope and Content of this work

The aim of the thesis is to understand the interaction between saturated hydrocarbons with noble metal surface. The importance of a detailed knowledge of surface processes at a molecular level will be emphasized. Different adsorbates at the metal surface relevant to catalytic partial oxidation of saturated hydrocarbons are characterized. The study is also carried out to identify the modification induced by the adsorption of numerous species on metal surface. Elementary reaction steps and their kinetic parameters for the surface reaction are evaluated to elucidate possible reaction mechanism. The applied method includes density functional calculations of complex chemical processes. These parameters build the starting point for detailed reaction mechanism on the catalytic surface in the future.

The thesis is structured as follows. In this Chapter viz. Chapter 1, the motivations behind the thesis and the aim of the thesis are summarized. In Chapter 2, the method used for our quantum chemical calculations is briefly described which includes computational details for the study. In Chapter 3, the adsorption of different radicals produced by saturated hydrocarbons has been studied. The nature and relative stability of each of the fragments has also been determined. The decomposition and fragmentation of ethane on a Rh(111) surface has been investigated. The possible reaction pathways with reaction intermediates are elucidated in detail. In Chapter 4, the dehydrogenation of propane on the Rh(111) surface has been studied which comprise of evaluating transition states of various elementary step reactions. In Chapter 5, possible reactions of the hydrocarbon fragments with oxygen which are relevant to catalytic partial oxidation have been investigated. In Chapter 6, the key results of this thesis have been briefly summarized with conclusive outlook.

# Chapter 2

# Method and Model

## 2.1 Quantum Mechanics

Isaac Newton and many contemporary 17th century scientists and philosophers had begun the classical mechanics which was believed to be a powerful and universally valid tool for describing nature completely. It accurately predicted the motion of planets and hence was believed to have enormous range of scale. At the beginning of 20th century, a scientific revolution took place in which classical Newtonian mechanics was found to be inadequate for explaining phenomena at a very small scale and a new theory was needed to explain behavior of energy and matter at atomic and subatomic level. This is how quantum mechanics came into picture and is considered to be one of the great ideas of the 20th century. Quantum mechanics [18] is very successful in describing the behavior of very small (atomistic and sub-atomistic range) systems, which the Newtonian mechanics fails to describe.

In 1900, Max Planck deduced the distribution law for black body radiation and the concept of quantization first came into consideration. Then in 1913, Niels Bohr made the first attempt to apply quantum theory to dynamical system by calculating the energy levels of atomic hydrogen. In 1923, Louis de Broglie proposed that particle-like objects, such as electrons, could also behave like a wave and in 1926, Davisson and Germer observed the electrons experimentally. In 1926, Schrödinger developed the basic equation of quantum mechanics.

Today theory of quantum mechanics is applied to understand the behavior of atomic particles and provides the foundation for understanding various phenomena especially in natural science. It is also successful to describe precisely the complex processes occurring in real systems. The main difficulty with the theory is that the underlying equations in quantum mechanics are quite complicated to be solved analytically for all the systems. But, fortunately due to continuous development of various computational methods, it is practically possible for the present day scientists to treat bigger system (for example a system containing 100 atoms or larger) and solve the equations numerically by modeling the real processes of interest computationally in an optimized manner.

### 2.1.1 Schrödinger Equation

The theory of quantum mechanics is built upon the fundamental concepts of wave-functions and operators. The wave-function is a single-valued square-integrable function of the system parameters and time which provides a complete description of the system. In 1926, Austrian physicist Erwin Schrödinger developed a wave equation in terms of the wavefunction which predicts analytically and precisely the probability of events or outcome.
Time-dependent Schrödinger equation is given by:

$$i\hbar\,(\mathrm{d}\psi(r,t)/\mathrm{d}t) = -\,(\hbar^2/2m)\nabla^2\,\psi(r,t) + V(r)\,\psi(r,t)$$

$\Psi$ is the wave function; the probability amplitude for different configurations of the system at different times, $-\,(\hbar^2/2m)\nabla^2$ is the kinetic energy operator $T$, $V$ is the potential energy operator. The theory of the Schrödinger equation relies on the interpretation of the wave function in terms of probabilities. The absolute square of the wavefunction, $|\Psi(r,\,t)|^2$ is interpreted as the probability density

for finding a particle in the vicinity of $r$ at time $t$. For this to have physical meaning the wavefunction needs to be a well-behaved function of r and t. Therefore $\Psi$ should be a finite, single-valued, and continuous function.

Separation of variables is carried out for time dependent equation and thus we obtain the time independent Schrödinger equation, which is given by:

$$i\hbar\,(\mathrm{d}\psi(r)/\mathrm{d}t) = -\,(\hbar^2/2\mathrm{m})\nabla^2\,\psi(r) + V(r)\,\psi(r)$$

The equation defines the stationary wave solutions of the time dependent Schrödinger equation, which are the states with definite energy. The equation can also be represented as the following eigen value equation:

$$\hat{H}\Psi = E\Psi$$

Where, $E$ is the total energy of the system. To obtain specific values for energy, we operate on the wavefunction with the quantum mechanical operator $\hat{H}$ associated with energy and the operator is called Hamiltonian. Solutions exist for the time-independent Schrödinger equation only for certain values of energy, and these values are called eigenvalues of the energy. So, the Schrödinger equation, based on postulates of quantum mechanics represents a time dependent equation which can be further reduced to a time independent equation that is very useful for calculating energy eigenvalues.

### 2.1.2 Born Oppenheimer Approximation

In atoms, nuclei are much more massive than the electrons; so, they must accordingly have much smaller velocities. Thus, while solving the time-independent Schrödinger equation, one can assume that the nuclei are stationary and solve for the electronic ground-state first, and then calculate the energy of

the system in that configuration and solve for the nuclear motion. This separation of electronic and nuclear motion is known as the Born-Oppenheimer approximation [19].

Molecular wave function in terms of electron positions $r_i$ and nuclear positions $R_j$ can be expressed as:

$$\Psi_{\text{molecule}}(r_i, R_j) = \Psi_{\text{electrons}}(r_i, R_j)\,\Psi_{\text{nuclei}}(r_i, R_j)$$

By the approximation, the electronic Schrödinger equation is solved, yielding the wavefunction $\Psi_{\text{electrons}}$ depending on electrons only.

$$\hat{H}_{\text{electrons}}\Psi_{\text{electrons}}(r_i, Rj) = E_{\text{electrons}}\Psi_{\text{electrons}}(r_i, R_j)$$

Without this approximation only small molecules could have been treated and thus this approximation becomes a very important tool of quantum chemistry to carry out calculations of molecular wavefunction for larger molecules.

### 2.1.3 Density Functional Theory

Density-functional theory (DFT) [20] enables us to swiftly tackle the many-body problems and obtain all of the ground-state properties of the electronic system as unique functional (functions of another function) of the ground-state electron density. DFT is an extremely successful approach for the description of ground state properties of metals, semiconductors, and insulators. It is extensively used to study bulk materials and it also treats successfully the complex materials such as carbohydrates, proteins or carbon nanotubes.

The foundation of DFT is strongly backed by the two Hohenberg-Kohn theorems. The first theorem states every observable of a stationary quantum-mechanical system can be calculated exactly from the ground-state electron

density. Hence the total energy is a unique functional of the electron density ρ(r) and is given by:

$$E = E[\rho(r)] = \int \rho(r)\, v_{\text{ext}}\,(r)\, \mathrm{d}r + \mathrm{F}[\rho(r)]$$

$E[\rho(r)]$ is the energy functional, $F[\rho(r)]$ is a universal functional of the electron density $\rho(r)$ but is unknown.

The second theorem states that the ground-state energy can be obtained variationally: the density that minimizes the total energy is the exact ground-state density.

From the first Hohenberg-Kohn theorem, if the energy functional would have been known, then the ground state electron density could have been easily be found using the second theorem hence requiring the variation of the energy functional with respect to the electron density to vanish. But the theorems give no information about how to construct the functional. Kohn and Sham then devised a simple method where they replace original many-body problem with an independent electron problem that can be solved.

## Kohn-Sham Equation

Though the Hohenberg-Kohn theorems put forward a revolutionary idea yet in practice, they do not offer a way of computing the ground-state density of a system. In 1965, Kohn and Sham [21] further developed a simple method combining the wave function approach and the electron density approach, for calculating the ground state energy as a functional of the electron density as solving a set of single particle Schrödinger equations. They introduced a fictitious system of non-interacting electrons moving in an effective potential chosen such that its ground state electron density is the same as the one of the true system.

The value of the energy functional for a given density $\rho(r)$ is given as:

$$E[\rho(r)] = T[\rho(r)] + \int \rho(r) \, [V_{ext}\,(r) + V_{ee}(r)] \, dr + E_{xc}[\rho(r)]$$

where $T[\rho(r)]$ is the kinetic energy of non-interacting electrons, $V_{ext}$ is the potential from the nuclei, $V_{ee}$ is the classical coulomb electron-electron interaction. $E_{xc}$ $[\rho(r)]$ is called exchange-correlation functional and it takes into account all the contributions that were not considered in previous terms like electron exchange, electron correlation and correction needed for the kinetic energy and electron-electron interaction energies.

The density obtained when solving the alternative non-interacting Kohn-Sham equation is the same as the exact ground-state density. The ground-state density is thus obtained by solving the $N$ one-electron Schrödinger equations.

$$[-1/2 \, \nabla^2 + v_{KS}(r)] \, \Psi_i(r) = \varepsilon_i \Psi_i(r)$$

The electron density $\rho(r)$ can be expressed in terms of Kohn-Sham orbitals $\Psi_i$ $(r)$ as:

$$\rho(r) = \sum_i \left| \Psi_i(r) \right|^2$$

The non-interacting kinetic energy $T[\rho(r)]$ is given by:

$$T_s[\rho(r)] = -1/2 \sum_{i=1}^{N} \int \Psi_i^*(r) \, \nabla^2 \, \Psi_i(r) \, dr$$

Rest of other terms contributing to the total energy functional $E[\rho(r)]$ are functionals of electron density. Kohn and Sham introduce the special term in a way that the unknown contribution to the total energy of the non-interacting system become as small as possible, and this is indeed the case with the

exchange-correlation energy, however it is still an crucial contribution since the binding energy of many systems is about the same size as exchange-correlation functional, so an accurate description of $E_{xc}[\rho(r)]$ is important for the prediction of binding properties.

## Exchange-Correlation Functional

First simple approximation for evaluating exchange and correlation functional is the local density approximation (LDA) [22] which locally substitutes the exchange-correlation energy density of an inhomogeneous system by that of an electron gas evaluated at the local density. LDA functional has the form given by:

$$E_{xc}[\rho(r)] = \int \varepsilon_{xc}[\rho(r)]\rho(r)\mathrm{d}r$$

While many ground state properties (e.g., lattice constants, bulk modulas) are well described in the LDA, the calculation carried out for the molecular bond energies, cohesive energies of solids and binding energy on surfaces are often overestimated. The dielectric constant is overestimated by up to 40% in LDA compared to experiment.

It is observed that the exchange-correlation energy $\varepsilon_{xc}[\rho(r)]$ is not only influenced by the local density but also by the gradient of electron density and this approximation is known as generalized gradient approximation (GGA) [23]. GGA functional form is described as:

$$E_{xc}[\rho(r)] = \int \mathrm{f}[\rho(r), \nabla\rho(r)]\rho(r)\mathrm{d}r$$

Practical applications of DFT are thus based on approximations for the exchange-correlation potential. The exchange-correlation potential describes the effects of the Pauli principle and the Coulomb potential beyond a pure electrostatic

interaction of the electrons. There is continuous development for the approximations for the exchange-correlation energy to obtain improved exchange-correlation functionals.

We have used exchange and correlation functional proposed by Perdew and Wang [23] for all our calculation for Rh surface.

## 2.2 DFT as Implemented in Codes

In this thesis the plane wave DFT calculations are performed using CASTEP (Cambridge Sequential Total Energy Package) and VASP (Vienna Ab-initio Simulation Package). CASTEP is commercially available software from Accelrys. The description is mentioned in a previous thesis [24] and is summarized below. VASP is the software from University of Vienna and mostly used in molecular modeling for research purpose. The parallel version of VASP is very useful for calculation of large systems in an economic way.

### 2.2.1 CASTEP

CASTEP [25-26] is an *ab initio* quantum mechanical program which employ density functional theory (DFT) to simulate the properties of solids, interfaces, and surfaces for a wide range of materials classes such as ceramics, semiconductors, and metals. CASTEP is developed in the Theory of Condensed Matter Group at Cambridge University, UK. It is a suite of programs that provides advanced quantum mechanical calculations for chemicals and materials research.

CASTEP utilizes total energy plane-wave pseudopotential method where ionic potentials are replaced with effective potentials which acts only on the valence electrons in the system. Electronic wavefunctions are expanded through a plane wave basis set and exchange and correlation effects in electron- electron interactions can be included within either the local density (LDA) or generalized gradient (GGA) approximations. Combining the use of pseudopotentials and

plane wave basis sets makes it easier to calculate the forces on the atoms, enabling efficient optimization of ionic configurations of molecules, solids, surfaces, and interfaces. CASTEP takes the number and type of atoms in a system and predicts properties such as lattice constants, molecular geometry, elastic constants, band-structures, density-of-states, charge densities and wave functions, and optical properties.

### 2.2.2 VASP

The Vienna Ab-initio Simulation Package (VASP), is a package for performing ab initio quantum mechanical molecular dynamics (MD) using either Vanderbilt pseudopotentials, or the Projector Augmented Wave (PAW) Method, and a plane wave basis set. VASP was originally developed at the University of Technology of Vienna, Austria, in the group of Jürgen Hafner by Georg Kresse and Jürgen Furthmüller.

The interaction between ions and electrons is described using ultrasoft pseudopotentials (US-PP) or the projector augmented wave method and both techniques allow a considerable reduction of the necessary number of plane-waves per atom for transition metals and first row elements. Forces and stress can be easily calculated with VASP and used to relax atoms into their instantaneous ground state.

## 2.3 Supercell Approach

The supercell method imposes a periodicity on the simulation cell to model the continuum properties of the system better. For example a crystal surface may be represented by a finite length slab periodically repeated in 3 dimensions or to study a molecule, it can be put in a box and repeated periodically to be treated as periodic system. There is no limitation on the shape of supercell, however, the

supercell chosen must be large enough so that the spurious interactions are small between periodic images.

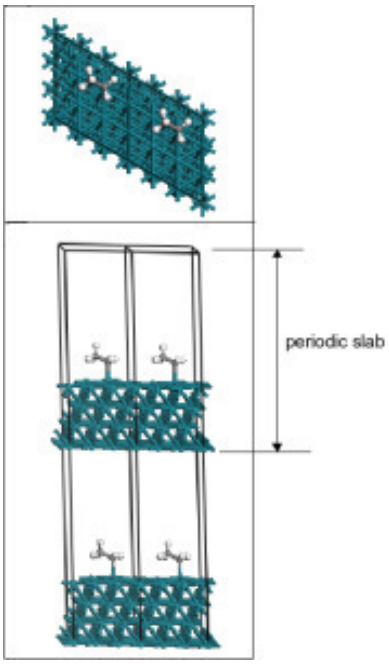


**Fig 2.1.** Periodic unit cell repeated in horizontal and vertical direction, top panel: top view, bottom panel: side view

A vacuum layer between top layer of one slab and bottom layer of the next periodic slab is placed to minimize vertical interactions and thus the supercells approximate aperiodic system to a periodic one. The limitation for supercell approach is that the supercell must be neutral charged as the electrostatic energy of an infinite charged system diverges.

## 2.4 The Plane-Wave Basis Set

Plane wave calculations using periodically repeated supercell geometries now make up the majority of DFT calculations in the area of surface science and heterogeneous catalysis. The plane wave basis sets are popular in calculations involving periodic boundary conditions for three dimensional systems. The

electronic wave functions at each *k*-point can be expanded in terms of discrete plane-wave basis set is given by Bloch's theorem.

Using Bloch's theorem [27-29], the wavefunction can be written as a product of a cell periodic part $u_i(r)$ and a wavelike part $e^{ik.r}$ with the wave vector k,

$$\Psi_i(r) = u_i(r).\, e^{ik.r}$$

u(r) can be expanded as a set of finite number of plane waves whose wave vectors are reciprocal lattice vectors of the crystal

$$u_i(r) = \sum_G c_{i,G}.e^{iG\cdot r}$$

Where, *G* are reciprocal lattice vectors and $c_{i,G}$ represent the expansion coefficients.

Thus the electronic wave functions can be written as sum of plane waves,

$$\Psi_i(r) = \sum_G c_{i,G}.\, e^{i(k+G)\cdot r}$$

In a periodic system, the infinitely extended integrals in real space over the system are replaced by the finite integrals over the Brillouin zone in reciprocal space by virtue of Bloch's theorem. This issue is dealt with by sampling the Brillouin zone at special sets of *k*-points.

The coefficients for the plane waves with small kinetic energies are more important than larger ones and hence the plane wave basis set can be reduced to include only those plane waves that have smaller kinetic energies than certain cut-off energy. The reduction of basis set at finite cut-off energy can lead to an error in the calculated total energy but it is possible to reduce the error by

increasing the cut-off energy value. Cut-off energy can be increased until the calculated total energy converges within the required tolerance.

The set of plane waves is restricted to a sphere in reciprocal space most conveniently represented in terms of a cut-off energy $E_{cut\text{-}off}$ such that for all values of $G$:

$$\{\hbar^2 \left| G + k \right|^2\}/2m \leq E_{cut\text{-}off}$$

Thus, the convergence of the calculation with respect to basis set may be ensured by variation of a single parameter, $E_{cut\text{-}off}$ . This is a significant advantage over many other basis set choices, with which calculated properties often show extreme sensitivity to small changes in basis set and no systematic scheme for convergence is available. In case of plane wave basis sets, same basis set can be used for all atomic species, convergence toward completeness can easily be tested and plane waves do not depend on nuclear positions and therefore correction terms are not needed for the calculation of forces.

## 2.5 Pseudo-Potentials

Plane-wave basis sets are often used in combination with an effective core potential or pseudopotential, so that the plane waves are only used to describe the valence charge density. This is because core electrons tend to be concentrated very close to the atomic nuclei, resulting in large wavefunction and density gradients near the nuclei which are not easily described by a plane-wave basis set unless a very high energy cut off, and therefore small wavelength, is used. The pseudopotential approximation exploits this by removing the core electrons and combining the interaction between the core and valence electrons and the strong nuclear valence electron interaction into a weaker pseudopotential. A schematic representation of pseudopotential method is given fig 2.2.

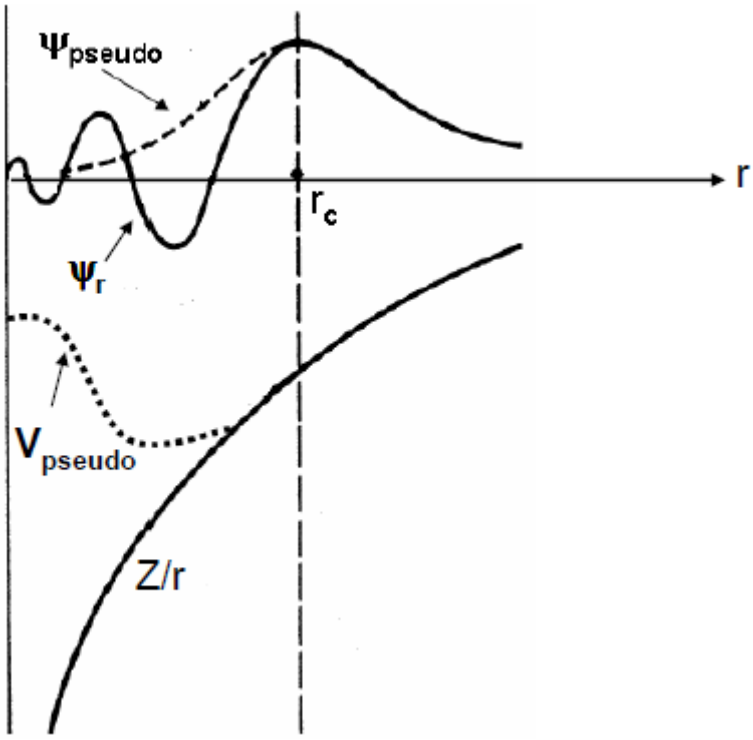


**Fig 2.2.** The Pseudopotential approximation

Ultrasoft pseudopotentials used in plane wave calculations describe the core electrons of atoms and enable plane wave basis set calculations with very low cut-off energy. However, a lot of calculations are carried now a days using projector augmented wave (PAW) method, which further reduces the expense of calculation. In most cases, both approaches have similar result however there are few exceptions e.g. transition metals with large magnetic moments and alkali metals [30].

## 2.6 Brillouin-Zone Sampling

By the use of Bloch's theorem, the plane waves with infinite number of electrons thus can be expressed as the wavefunction in terms of an infinite number of reciprocal space vectors within the first Brillouin zone of the periodic cell. So, Brillouin zone sampling at special sets of *k*-points is carried out. The k-points at

which the Brillouin zone is to be sampled during a self consistent calculation to find the electronic ground state is given by many methods [31-33], in the present study it is described by Monkhorst-Pack grid [32] in terms of the dimensions of the k-point mesh or a minimum k-point density. The number of k-points along each coordinate is determined by three integer values of $q_i$. The integers generates a sequence of numbers according to

$$u_i = (2r - q_i - 1) / 2\, q_i$$

where r varies from 1 to $q_i$ and $i$ represents the coordinates in reciprocal space $x$, $y$, $z$. Monkhorst-Pack scheme gives the grid size such as $k$ is distributed homogeneously in Brillouin zone as:

$$k_{xyz} = u_x z_1 + u_y z_2 + u_z z_3$$

where $z_1$, $z_2$ and $z_3$ are the lattice vectors in reciprocal space. The computational effort could be reduced by using a carefully chosen k-point set.

## 2.7 Geometry Optimization

Geometry optimization is carried out to find minima on the potential energy surface to get equilibrium structures. Optimization to minima is also known as energy minimization. Commonly geometry optimization technique is used to obtain a structure for a single-point quantum mechanical calculation, which provides a large set of structural and electronic properties. It is also used to prepare a structure for molecular dynamics simulation.

During geometry optimization, the cell parameters and the atomic coordinates are varied iteratively until a stable structure is obtained corresponding to the minimum force and stress for which convergence tolerance is defined.

In a surface chemical process, after optimizing the geometry of the molecule in the surface, adsorption energy can be calculated. For calculation of adsorption energy $E_{ads}$, the slab is geometry optimized with the species added to the slab and also only slab without the species. The geometry of the species was optimized within a cell similar to the cell of the slab and the energy of this optimized surface species was calculated subsequently. The energies of the optimized slab with and without species were calculated subsequent to the geometry optimization. The adsorption energies were determined according to:

$$E_{\text{ads}} = E_{(\text{slab + species})} - (E_{\text{slab}} + E_{\text{species}})$$

Negative adsorption energy indicates a stable adsorption and the positive adsorption energy indicates that the species is stable in gas phase.

## 2.8 Transition State Search

Transition state search determines the structure and energy of transition state in chemical reactions and also calculates barrier height in a diffusion process.

The structures of reactants and products were relaxed prior to calculating activation energies as well as reaction heats for the particular reaction. The transition state of the reaction was located on the potential energy hypersurface by performing a linear synchronous transit (LST) combined with a quadratic synchronous transit (QST) calculation and conjugate gradient refinements [21]. The total energies for reactants, transition state, and products were computed. Heats of reaction were calculated according to:

$$\Delta E_{\text{reaction}} = \Delta E_{\text{reactants}} - \Delta E_{\text{products}}$$

and the activation energy is calculated according to

$$E_{\text{act}} = \Delta E_{\text{transition State}} - \Delta E_{\text{reactants}}$$

## 2.9 Computational Details

All of our calculations for the chemical problems mentioned in this thesis have been made by means of state of art DFT using the code CASTEP and VASP. Various lateral sizes of supercells were chosen for studying molecules on Rh surface. The depth of slab for each calculation is taken as 4 layers. A vacuum slab of 10 Å is chosen for $C_1$ species, 12 Å for $C_2$ species and 15 Å for $C_3$ species in the corresponding slab. In the present work, to account for exchange and correlation functional the generalized gradient approximation as proposed by Perdew and Wang (PW91) has been applied as it is established that this approximation for the functional gives accurate description of chemical surface processes. In all the calculations, k-points spacing was set to 0.05 Å within the Brillouin zone as generated by Monkhorst-Pack scheme. The plane wave pseudopotential approach combined with k-point sampling results in time saving and accurate calculations. Where required, we took into account spin polarization. All the parameters are checked for their sensitivity and the variation in measured quantity like adsorption energies of less than 2% were obtained from the optimized one.

# Chapter 3

# Ethane Dehydrogenation and Fragmentation on a Rh(111) Surface

## 3.1 Introduction

Fundamental understanding of hydrocarbon reactions on metal surfaces is of immense importance in heterogeneous catalysis. A large number of industrially relevant processes such as catalytic partial oxidation [1, 2, 34], catalytic steam cracking [35], Fischer-Tropsch synthesis [36, 37] and alkene hydrogenation [38, 39] are crucially influenced by the stability and reactivity of hydrocarbon fragments at metal surfaces. Despite the high performance of various spectroscopic techniques like IR, SFG, TOF-SIMS, the low concentrations and short lifetimes of reaction intermediates make their identification quite cumbersome and challenging. For the determination of the structural properties of these reactive species along with the thermodynamic and kinetic parameters of their elementary reactions, state-of-the-art DFT is becoming increasingly popular in many branches of science, particularly in the area of surface science. Specifically, theoretically predicted energies can serve as the fingerprints for the characterization of reactive intermediates.

Ethane is the simplest saturated hydrocarbon having a C-C bond and is consequently an appropriate model species in order to study the conversion of

higher hydrocarbon to synthesis gas. Many experimental and theoretical studies of the catalytic partial oxidation have been carried out on different catalytic surfaces using methane as model, however, in the comparison, only few studies have been carried out so far for the ethane combustion on noble metal surfaces. Therefore this system needs special attention to investigate the full chemistry of $C_2$ hydrocarbons on catalytic surfaces. For the choice of the catalyst amongst noble metals, Rh [1, 3, 4] is established to be the most selective one for the production of synthesis gas. In this chapter we discuss the theoretical investigation of the ethane dehydrogenation and dissociation on Rh(111) surface, which plays an important role in the development of reaction mechanism for the formation of synthesis gas.

To understand first step towards dissociative adsorption, there is an extensive interest in the possibility of activating C-H bonds present in alkanes by noble metal based catalysts. However, saturated hydrocarbons are expected to weakly interact with metal surfaces and consequently very few experimental studies have been reported on metal single-crystal surfaces [40]. Chesters group [41] reported the RAIRS spectra of ethane on Cu(111) at 91 K, which indicated weak distortion of the molecule upon interaction with the surface. Madix and coworkers [14, 42] used supersonic molecular beam techniques to investigate the adsorption of methane and ethane on Pt(110)-(1x2) surface at temperatures in the range of 500–1400 K. Interestingly, compared to a Pt(111) surface, these alkanes were found to adsorb by direct dissociation on Pt(110)-(1x2) surface with a relatively higher energy barrier. We have investigated the thermodynamics and kinetics of the dehydrogenation of ethane on Rh(111) for 0.11 ML coverage. Notably, owing to the increasing complexity of the adsorption system, studies for ethane on Rh surface have received much less attention than methane within the frame of the DFT community.

This chapter is aimed at mapping out the minimum energy pathway for ethane dehydrogenation and decomposition to $C_2$ and $C_1$ fragments using periodic

density functional theory calculations. Dissociative adsorption of ethane followed by dehydrogenation is found to be the primary step for the Catalytic Partial Oxidation of ethane. In this chapter, we also investigate the fragmentation of ethane on Rh(111). In a subsequent study in chapter 5, we will discuss the oxidation of $C_2H_x$ and $CH_x$ species relevant to the catalytic partial oxidation process. To understand the whole catalytic process of ethane dehydrogenation and decomposition, the geometries, binding energies, and binding site preferences for intermediate chemisorbed hydrocarbon species and hydrogen are determined and rationalized to provide insights into the elementary reaction steps as detailed below.

## 3.2 Adsorption of Ethane

The first step in heterogeneous reactions is the adsorption of reactant gas molecules on the surface. Hence, a fundamental understanding of surface reactivity requires the examination of the critical factors that govern the adsorption process. In order to understand the C-H bond activation of ethane, its dissociative chemisorption is studied to predict correctly the reactivity of the molecule on Rh surface. We explored several adsorption sites (top, bridge, hollow) for molecular ethane on the clean Rh(111) surface. As expected, ethane does not show much sensitivity to site preference according to our DFT calculation. In the bridge adsorption mode the C–C bond axis is aligned along a Rh–Rh bond whereas in the top structure the C–C midpoint is above a Rh surface atom. The bridged configuration is found to be most stable and the binding energy is calculated to be 0.32 eV. $C_1$-Rh distance and $C_2$-Rh distance is calculated as 3.50 and 3.58 Å respectively. These surface structures and are in good agreement with those predicted from experiments [43]. Ethane is found to adsorb molecularly on the terrace sites of Pt(111) at 95 K with a saturation coverage of ca. 0.3 monolayer and desorbs at ca. 132 K during TPD studies [44].

## 3.3 Adsorption of $C_2H_x$ (x=0-5) Species

We obtained the adsorption modes and the corresponding adsorption energies for all $C_2H_x$ (x=0-6) species on a 3x3 unit cell. **Fig 3.1** shows the geometry of the intermediate structures involved in the reaction. The reaction intermediate species are ethyl ($C_2H_5$), ethylidene ($CH_3CH$), ethylene ($CH_2CH_2$), ethylidyne ($CH_3C$), vinyl ($CH_2CH$) and Acetylene (CHCH). Other intermediates such as vinylidene ($CCH_2$), ethynyl (CCH) and carbidic ethynylene (CC ) species are also identified. A detailed knowledge of the chemisorption of hydrocarbon species on the rhodium surfaces is useful to gain some insight into understanding the corresponding catalytic processes.

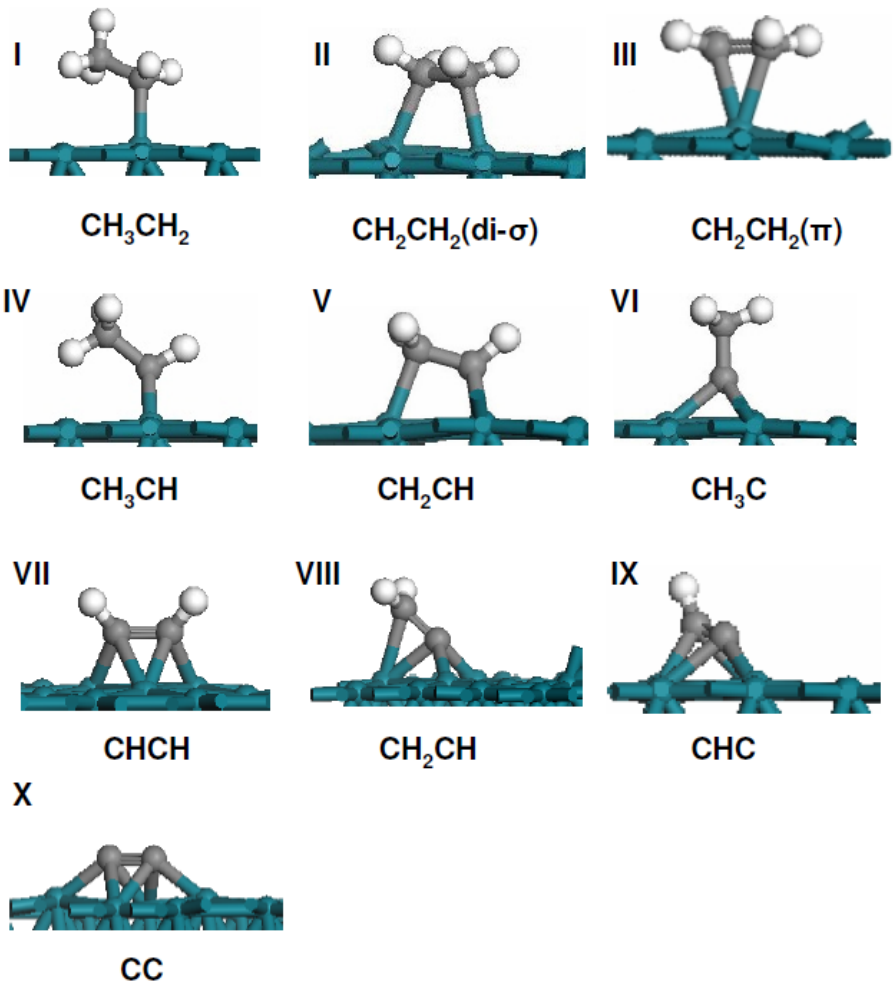


**Figure 3.1** Surface radicals involved in the dehydrogenation of ethane

Ethyl Adsorption: Ethyl ($C_2H_5$) radical is found to prefer atop adsorption where the surface metal atom essentially replaces the hydrogen atom of ethane in order to form a surface intermediate resembling like ethane preserving its $sp^3$ symmetry. On adsorption, the C-C bond axis was found to tilt upward somewhat with respect to the surface plane. The C-C bond distance is 1.51 Å, which is slightly shorter than the 1.53 Å calculated for free $C_2H_6$ in the gas phase. The binding energy of 2.10 eV is calculated for ethyl species on a Rh(111) surface. The adsorption site preference is attributed to the balance between the Pauli repulsion and the orbital overlap according to Hoffmann [45] and Schustorovich and Baetzold [46] orbital interaction scheme.

Ethylidene Adsorption: Ethylidene ($CH_3CH$) is found to show preference towards bridge site so that C-atom lies between two vicinal metal atoms and is bonded in such a way to satisfy valence rule for sp3 hybridization. The binding energy is calculated as 4.33 eV. The C-C bond of the adsorbed ethylidene is 1.5 Å and the two C-Rh bond lengths are determined to be 2.05 Å and 2.06 Å.

Ethylene Adsorption: We observe that ethylene ($CH_2CH_2$) adsorbs on a Rh(111) surface by binding to an bridge site leading to a di-σ bonded ethylene where two carbons atoms are bonded covalently to the adjacent Rh atoms and each C has the binding of $sp^3$-hybridized orbitals, as expected. The C-C bond is found to be 1.47 Å, clearly indicating a σ-bond formation. A di-σ ethylene geometry, has been previously reported experimentally on Pt(111) using HREELS [47], UPS [48] and NEXAFS [49]. The next most energetically stable structure of ethylene observed involves the hydrocarbon species forming a π-bonding on to the surface at a top site. The C-C bond length observed is 1.40 Å with the C-Pt bond at 2.19 Å and 2.18 Å. A similar structure of the π-coordinated ethylene is also observed on Pt(111) [50] and Pd(111) [51] surface where the corresponding C-C bond length

calculated is 1.41 Å and 1.38 Å with the C-Pt bond length as 2.12 Å and 2.20 Å respectively. The adsorption energies are calculated to be 1.04 eV for the di-$\sigma$ bonded structure and 0.98 eV for the π-coordinated configuration of the ethylene molecule.

Vinyl Adsorption: We find that vinyl ($CHCH_2$) prefers to bind to an 3-fold site on Rh(111) surface with two Rh-$C_1$ bonds of 2.06 Å and 2.07 Å on one Rh-atom and another Rh-$C_2$ bond of 2.11 Å on neighboring Rh-atom. The molecule has each C-atom having four bonds as expected for a $sp^3$-configuration and carbon-carbon is a σ-bond. The calculated binding energy for hexagonal close-packed hollow (hcp) site is found to be 2.99 eV and is preferred over fcc site by 0.10 eV. The C-C distance is 1.45 Å and is stretched by 0.15 Å as compared to 1.30 Å for free vinyl in gas phase. The binding energy of vinyl on Rh(111) is found to be 3.04 eV.

Ethylidyne Adsorption: On Rh(111), ethylidyne occupies a hcp site where there is a Rh-atom from the second metal layer directly under the carbon that is bound to the metal surface. The binding energy of vinyl on Rh(111) is found to be 6.34 eV. Ethylidyne has been detected spectroscopically as stable surface species and extensive studies has been carried out to elucidate the structure of ethylidyne on Rh(111) [52-56], Pt(111) [56-58], Pd(111) [56, 59, 60], Ir(111) [61], and Ru(0001) [62] and it is observed to potentially adsorb in three fold sites . Ethylidyne on Pt(111) occupies the threefold fcc metal site with its C–C bond is normal to the metal surface whereas on Rh(111) it prefers hcp occupancy and the different site occupancy of ethylidyne on the Rh(111) surface changes the nature of adsorbate induced restructuring of the metal surface around the chemisorption bond as reported by LEED crystallography.

Accetylene Adsorption: Accetylene (CHCH) is found to adsorb on Rh(111) surface most preferably in parallel bridged position with an adsorption energy of

2.64 eV. Each C-atom of HC-CH is bridged between two neighboring Rh atoms with C-Rh distance as 2.03 Å and 2.17 Å. The C-C bond distance is calculated to be 1.38 Å and it is noticed that the bond is elongated after adsorbing to surface by 0.18 Å as compared to free ethyne in the gas phase. Experimental studies on Pd(111) [63] found that ethyne adsorbed at a surface temperature of 120 K is converted to vinylidene at 213 K. It was also observed by supersonic molecular beam technique that the stable dissociation product of ethane on Pt(110) [64] at all coverages to have $C_2H_2$ stoichiometry in the surface temperature range 350-400 K. This species then found to decompose above 400 K to $C_2H$.

Vinylidene Adsorption: Vinylidene species is a two-electron donor and can act as a terminal or bridging ligand while forming stable complexes with transition metals [65]. The binding energy of vinylidene on Rh(111) is calculated as 4.40 eV on a hcp site, which is higher by 0.14 eV more stable than the corresponding fcc site. The $-CH_2$ fragment of $C-CH_2$ lies over a Rh atom like on top surface site, with a C-Rh bond length of 2.27 Å and the –C fragment is oriented in such way that the corresponding C-Rh bond lengths are found to be 1.99 Å, 1.99 Å and 2.09 Å. The C-C bond is calculated to be 1.39 Å long and is slightly elongated as compared to C-C bond of $C-CH_2$ in the gas phase which is 1.34 Å and thus suggests that the back-bonding is not as significant as in the case for acetylene.

Ethynyl Adsorption: Ethynyl (CCH) is found to be adsorbed on Rh(111) with the tertiary carbon atom located in a threefold site with an C-Pd distance of 1.97 Å, 2.11 Å, 2.10 Å and the -CH fragment lies while bonding two Pd atoms like bridged site and the C-Pd distance in this case is found to be 2.24 Å and 2.19 Å. The binding energy calculated to be – 4.78 eV. STM and NEXAFS experiments carried out for ethynyl species have reveal that the orientation of ethynyl adsorbed on Pd(110) is the [001] direction and the inferable adsorption site is the $\mu$-bridge site [66]. Theoretical study on Pd(111) report a structure where η2η3 (C,

C) structure where average C-Pd distance from –C of C-CH is 1.99 Å and from -CH fragment is 2.13 Å [67].

Carbidic Ethylene Adsorption: Each carbon atom in carbidic ethynylene (CC) bonds to the surface at a threefold site and C-C bond length is found to be 1.36 Å. The barrier for C-C bond scission of CC species is expected to be much higher than for any of the C-H bonds and also higher than C-C bond of other intermediate species. Experimental findings on ethane dehydrogenation on Pt(100) reported that a carbidic species is formed when the surface temperature is above 600 K and upon increasing the temperature further to 800 K, formation of carbonaceous multilayers or graphite takes place [64]. According to our theoretical investigation, we observe the formation of carbon species taking place as final decomposition product of ethane in the absence of oxygen.

**Table 3.1** shows the most stable identified adsorption configurations and adsorption energy of intermediate radicals involved in the decomposition of ethane.

| Radicals | $E_{ads}$ | $d_{C-Rh}$ | $d_{C-C}$ |
|---|---|---|---|
| $C_2H_5$ | -2.10 | 2.10 | 1.51 |
| $CH_3CH$ | -4.33 | 2.06, 2.05 | 1.50 |
| $CH_2CH_2$ (di-σ-bonded) | -1.04 | 2.14, 2.13 | 1.47 |
| $CH_2CH_2$ (π-bonded) | -0.98 | 2.19, 2.18 | 1.40 |
| $CH_2CH$ | -3.04 | 2.06, 2.07; 2.11 | 1.45 |
| $CH_3C$ | -6.34 | 2.01, 2.02, 2.02 | 1.48 |
| CHCH | -2.64 | 2.03, 2.17, 2.03, 2.17 | 1.38 |
| $CH_2C$ | -4.38 | 2.27, 1.99, 1.99, 2.09 | 1.39 |
| CHC | -4.78 | 2.24, 2.19, 2.36; 1.97, 2.11, 2.10 | 1.36 |
| CC | -5.90 | 2.043, 2.14, 2.15, 2.13, 2.03, 2.14 | 1.36 |

**Table 3.1.** Geometrical parameters (in Å) and binding energies (in eV) of the intermediate radicals in their stable configuration.

## 3.4 Reaction Pathways and Activation Barriers

For developing reaction pathway, the reactions and rearrangement considered are C-H bond-breakage (dehydrogenation), C-H bond formation (hydrogenation), 1,2-H shift (isomerization), diffusion to different sites and C-C bond-breakage (fragmentation) through various intermediates of $C_2H_x$. In this section, we present the study and elucidation of the reaction path comprising of various elementary steps from ethane to ethylidyne and then to carbon. For each elementary reaction step, we then describe the transition state structures and the activation and reaction energies. Our theoretical results relate important aspects of the experimental findings for ethane decomposition on Rh(111).

Reaction pathway for ethane dehydrogenation and fragmentation is summarised in **Scheme 3.1.** We consider the C–C bond breakage during fragmentation of radicals.

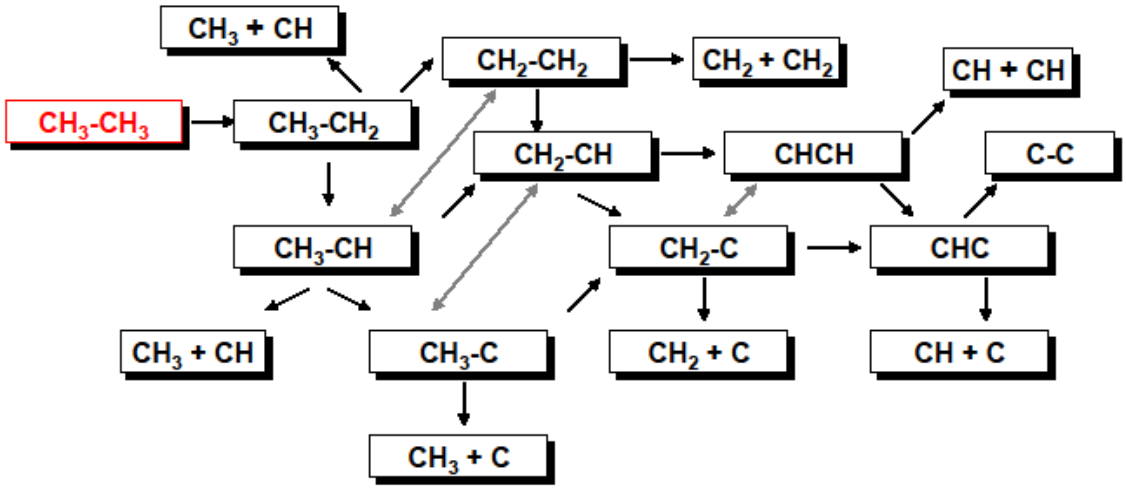


**Scheme 3.1.** Elementary paths for the dehydrogenation and fragmentation of ethane on Rh(111)

### 3.4.1 Ethane and $C_2H_x$ Dehydrogenation Reactions

Each elementary step is discussed in detail.

### 3.4.1.1 Ethane to Ethyl species formation

Ethane dissociative adsorption is followed by the formation of ethyl and hydrogen on catalyst surface. RAIR spectra of the primary products of the dissociative adsorption of ethane on a Pt(111) substrate at 150 K indicate that the ethyl moiety is formed by the reactive collision [67]. We study the dissociative adsorption of ethane to ethyl and hydrogen atom on Rh(111) surface. During the reaction, the $C_2H_6$ approaches towards one of two neighboring Rh atoms and bends towards the surface resulting $C_2H_5$ and H concertedly adsorbing on a atop site. On the same top site, the H is abstracted and simultaneously remains adsorbed at the transition state. The C-H bond of ethane is stretched to 1.80 Å. The H atom then moves to the neighboring fcc site. **Figure 3.2.a** shows the reactants and product structures along with transition state and **Figure 3.2.b** gives the energetics of the corresponding step.

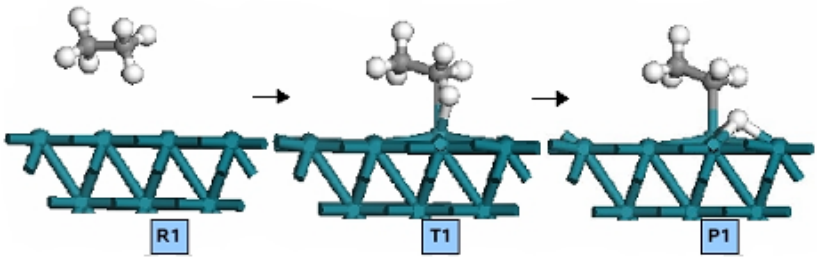


**Figure 3.2.a.** Dehydrogenation of $C_2H_6$ (reactant R1) to $C_2H_5$ and H (product P1) via transition state T1

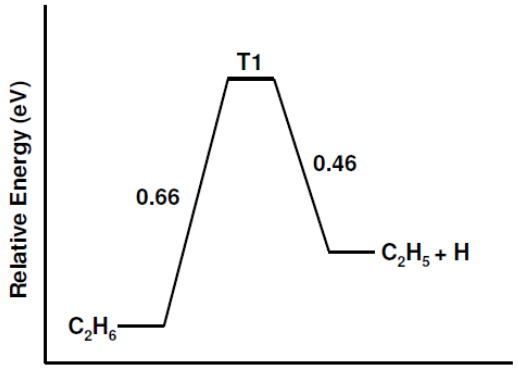


**Figure 3.2.b**. Energetics of the elementary step: $C_2H_6 \rightarrow C_2H_5$ and H

### 3.4.1.2 Ethyl to Ethylidene / Ethylene formation

A $C_2H_5$ species, which is stable when absorbed in a atop site on Rh(111) and can undergo two different dehydrogenation reactions. Abstraction of H from the low lying C-atom with respect to the catalyst surface, where the C-Rh distance is 2.10 Å leads to the formation of ethylidene and abstraction from methyl H of the other C-atom furnishes ethylene. Ethylene forms however with two adsorption configurations designated as di-$\sigma$ and $\pi$ bonded $CH_2CH_2$ on Rh(111). **Fig 3.3.a** and **Fig 3.3.b** show the structures and energy profile of the reactants, transition states and products for this reaction.

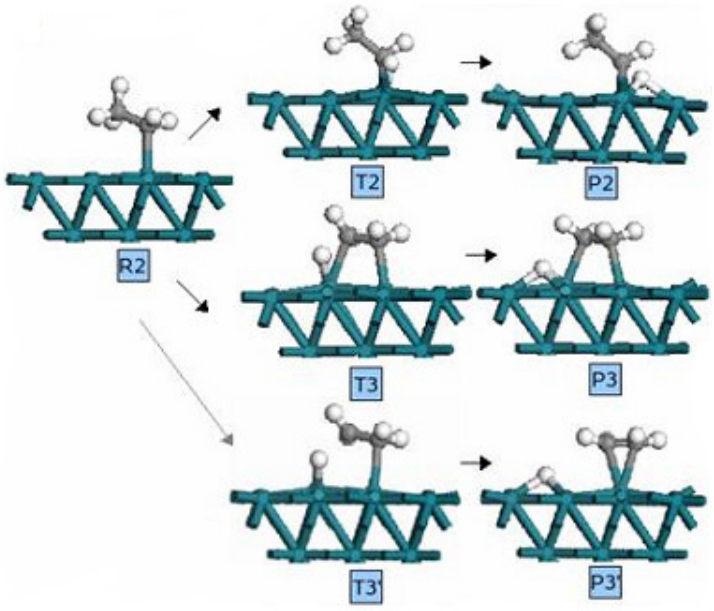


**Figure 3.3.a.** Dehydrogenation of $C_2H_5$ (reactant R2) to $CH_3CH$ and H (Product P2) via transition state T2 and to di-σ-bonded ethylene species and H (product P2) via transition state T3. Route to π-bonded ethylene species (product P3′) and H is shown via transition state T3.

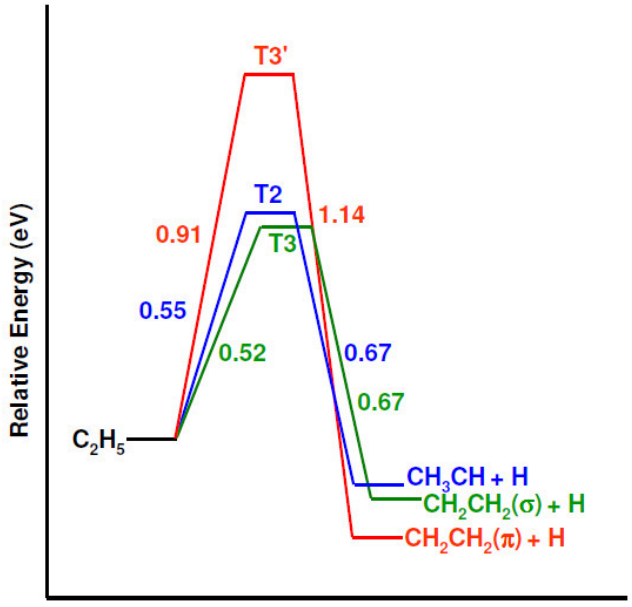


**Figure 3.3.b.** Energetics of the elementary steps $C_2H_5 \rightarrow CH_3CH + H$ and $C_2H_5 \rightarrow CH_2CH_2$ (di-$\sigma$ and $\pi$ bonded) + H

According to our DFT calculations, formation of ethylene and ethylidene from ethyl radical have comparable activation energies with a slight difference of 0.03 eV and both are expected to be prevalent at a particular temperature. Even though ethylidene is a transient intermediate species, experimental evidence indicates the formation of ethylidene from ethyl species on Pt(111) surface [67].

### 4.4.1.3 Ethylene to vinyl formation

Ethylene formed on Rh(111) surface is a stable species and undergoes dehydrogenation to form Vinyl species at the surface. In the transition state T4, dehydrogenation takes place from one of the methylidene moieties and the C atom relocates from the top site to a nearby bridge site forming C-Rh bonds at a distance of 2.24 Å and 2.18 Å. The H atom gets dissociated over the top of Rh atom, where the C-H distance being elongated to 1.62 Å and the H-Rh distance is observed to be 1.59 Å. The products formed are vinyl adsorbed at hcp site while the dissociated H atom occupies a nearby 3-fold site. The activation energy of the

elementary step is calculated to be 0.65 eV and the reaction is found almost thermoneutral. The structures for reactants, products and transition state are given in **Figure 3.4.a.** and the corresponding energy diagram is shown in **Figure 3.4.b.**

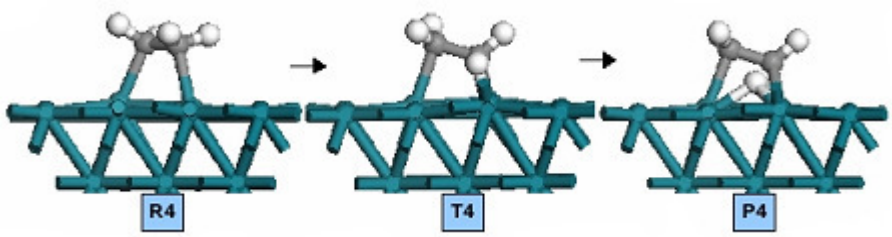


**Fig 3.4.a.** Dehydrogenation of $CH_2CH_2$ ( reactant R4) to $CH_2CH$ and H (Product P4) via transition state T4

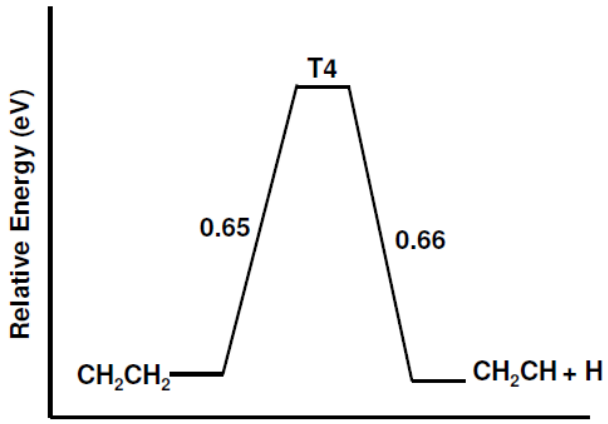


**Figure 3.4.b.** Energetics of the elementary step $CH_2CH_2 \rightarrow CH_2CH + H$

### 3.4.1.4 Ethylidene to Ethylidyne formation

Source of ethylidene on the surface is ethyl dehydrogenation, ethylene isomerization or vinylidene hydrogenation. Study of thermal chemistry of the ethyl moiety on Pt(111) surface using a combination of RAIRS and TPD, indicates that ethylidene ($CH_3CH$) intermediate is present in the dehydrogenation of ethyl to ethylidyne [67]. Ethylidyne on Rh(111) prefers the hcp metal site with its C–C

bond is normal to the metal surface and the nearest- and next- nearest neighbor metal atoms change their locations as compared with their positions on the metal surface before C–H bond dissociation occurs from $CH_3CH$. Experimental findings [68] confirm that ethylidyne formation from ethylene takes place even at low temperature of 150 K. The low barrier for the formation of ethylidyne from ethylidene is indeed remarkable, which indicates that the dehydrogenation is very fast and spontaneous. The structures for reactants, products and transition state are given in **Figure 3.5.a.** and the corresponding energy diagram is shown in **Figure 3.5.b.**

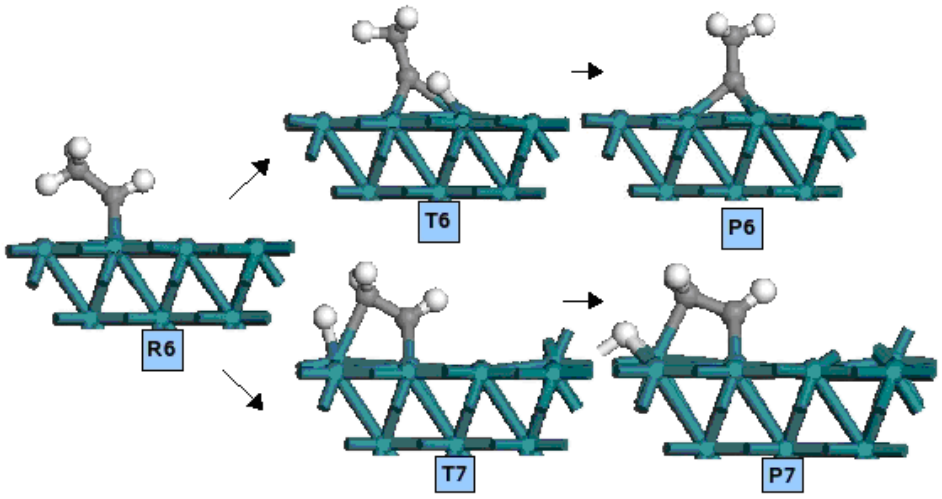


**Figure 3.5.a.** Dehydrogenation of $CH_3CH$ (reactant R6) to $CH_3C$ and H (Product P6) via transition state T6 and to $CH_2CH$ and H (product P7) via transition state T7.

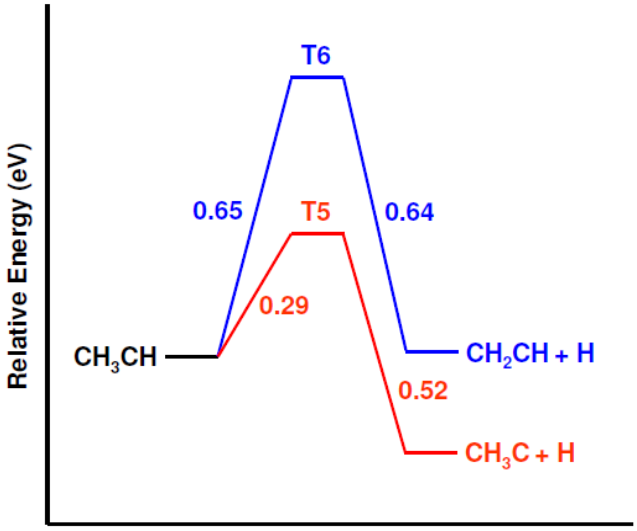


**Figure 3.5.b.** Energetics of the elementary steps $CH_3CH \rightarrow CH_3C + H$ and $CH_3CH \rightarrow CH_2CH + H$

We summarize the dehydrogenation reactions of ethane in **Table 3.2.**

| Dehydrogenation Reactions | Ea | ΔH |
|---|---|---|
| $CH_3CH_3 \rightarrow CH_3CH_2 + H$ | 0.66 | 0.20 |
| $CH_3CH_2 \rightarrow CH_3CH + H$ | 0.55 | -0.12 |
| $CH_3CH_2 \rightarrow CH_2CH_2$ (di-σ) + H | 0.52 | -0.15 |
| $CH_3CH_2 \rightarrow CH_2CH_2$ (π) + H | 0.90 | -0.23 |
| $CH_3CH \rightarrow CH_2CH + H$ | 0.65 | 0.01 |
| $CH_3CH \rightarrow CH_3C + H$ | 0.29 | -0.23 |
| $CH_2CH_2 \rightarrow CH_2CH + H$ | 0.65 | -0.01 |
| $CH_2CH \rightarrow CH_2C + H$ | 0.56 | -0.19 |
| $CH_3C \rightarrow CH_2C + H$ | 2.30 | 0.33 |
| $CH_2CH \rightarrow CHCH + H$ | 0.53 | 0.01 |
| $CHCH \rightarrow CHC + H$ | 1.42 | 0.63 |
| $CH_2C \rightarrow CHC + H$ | 2.55 | 0.90 |
| $CHC \rightarrow CC + H$ | 1.35 | 0.18 |

**Table 3.2.** Activation Barriers and Reaction Energies in eV for Dehydrogenation Reactions of $C_2H_x$ (x=0-5) Species on Rh(111)

### 3.4.2 $C_2H_x$ Isomerization Reactions

Vinyl to Ethylidyne formation

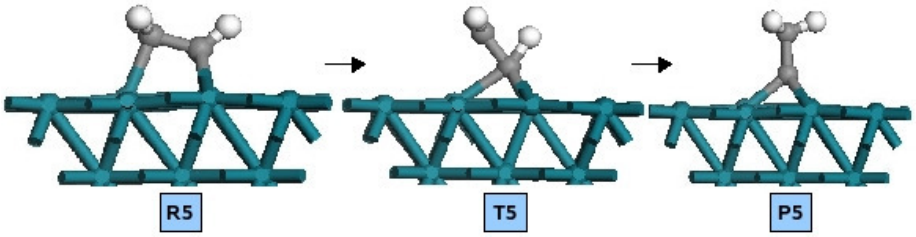


**Figure 3.6** Isomerization of $CH_2CH$ (reactant R5) to $CH_3C$ and H (Product P5) via transition state T5

The binding site preferences of ethylidyne find a different pace on Rh(111) than on Pt(111). Ethylidyne is found to adsorb on hcp hollow sites rather than the fcc hollow on Pt(111) and this different site occupancy of ethylidyne on the Rh(111) surface changes the nature of adsorbate induced restructuring of the metal surface around the chemisorption bond, as shown by LEED crystallography [56]. 1,2 shift reactions are considered for ethylene to ethylidene formation, vinyl to ethylidyne formation and vinylidene to acetylene formation. 1,2 shift of H from ethylene to form ethylidene is understood to be one of the initial steps for the formation of ethylidyne on noble metal surfaces [69-72]. Carter and co-workers [73] perform theoretical estimates of surface reaction energetics which indicate that ethylidene is energetically more favourable than ethylidyne in the presence of coadsorbed hydrogen. These authors also predict that ethene first isomerizes to ethylidene, while desorption of hydrogen around 300 K steers the subsequent reaction from ethylidene to ethylidyne. In contrast, our studies indicate that on Rh(111), 1, 2 hydrogen-shift reactions of adsorbed di-σ-bonded ethylene species have relatively high activation energies in comparison with hydrogenation and dehydrogenation reactions and are hence ruled out. In this

reaction the H-atom is transferred in the gas phase and the isomerization does not occur via surface.

According to experimental studies, vinyl intermediate as precursor of ethylidyne is not found to be favourable because vinyl species were shown to convert back to ethylene before producing ethylidyne on Pt(111) [74]. Vinyl isomerization to ethylidyne on Rh(111) is also found to be highly activated reaction according to our DFT calculations. This reaction also proceeds without involvement of surface Rh atom and the activation energy is found to be 2.15 eV.

Another isomerization reaction for the formation of acetylene from vinylidene is considered on Rh(111) surface. NMR studies of acetylene adsorption on Pt(111) showed the existence of $CCH_2$ and HCCH on the surface with a ratio of about 3:1 at 280 K, indicating that $CCH_2$ is more stable on the Pt(111) surface [75].

We summarize isomerization reactions of $C_2H_x$ in **Table 3.3**

| Isomerization Reactions | Ea | ΔH |
|---|---|---|
| $CH_3CH \rightarrow CH_2CH_2$ | 2.24 | -0.29 |
| $CH_3C \rightarrow CH_2CH$ | 2.69 | 0.66 |
| $CH_2C \rightarrow CHCH$ | 2.44 | -0.22 |

**Table 3.3.** Activation barriers and reaction energies in eV for isomerization reactions of $C_2H_x$ species on Rh(111)

### 3.4.3 $C_2H_x$ Fragmentation and Further Reactions

C-$CH_3$ being very stable at the surface, its further reaction is studied in detail to establish the mechanism for its decomposition on Rh(111) surface. C-$CH_3$ is adsorbed in hcp site and for the adsorption site, two different azimuthal orientations have been taken into account, C–H bonds pointing towards the nearest- neighbor Rh atoms and C–H bonds pointing midway between two

neighboring Rh atoms in the top layer. Diffusion to fcc site is not that prevalent due to comparatively high barrier of 0.50 eV.

Direct dissociation of C-C bond which stays almost perpendicular to the surface with a tilt of $2^0$ with the surface normal is studied and the reaction is found to be activated by 2.10 eV. In the transition state C-C bond is stretched to 2.67 Å and get titled in a fashion that the lower lying carbon atom stays back at the hcp site slightly driven towards bridged site and the above lying C of $CH_3$ moves to the top site of the nearby Rh atom. Finally the C atom migrates to the neighboring fcc site. Another competing reaction is the dehydrogenation reaction from any of the three equivalent methylidyne H present in the molecule. The activation energy of dehydrogenation reaction is calculated as 2.30 eV. Upon dehydrogenation, the dehydrogenated ethylidyne species is rearranged to form the Vinylidene species, which remains on its most preferred hcp site and the dissociated H atom migrates to the nearby hcp site. Both the fragmentation and dehydrogenation reactions are highly activated and only feasible at high temperature as suggested by experiments.

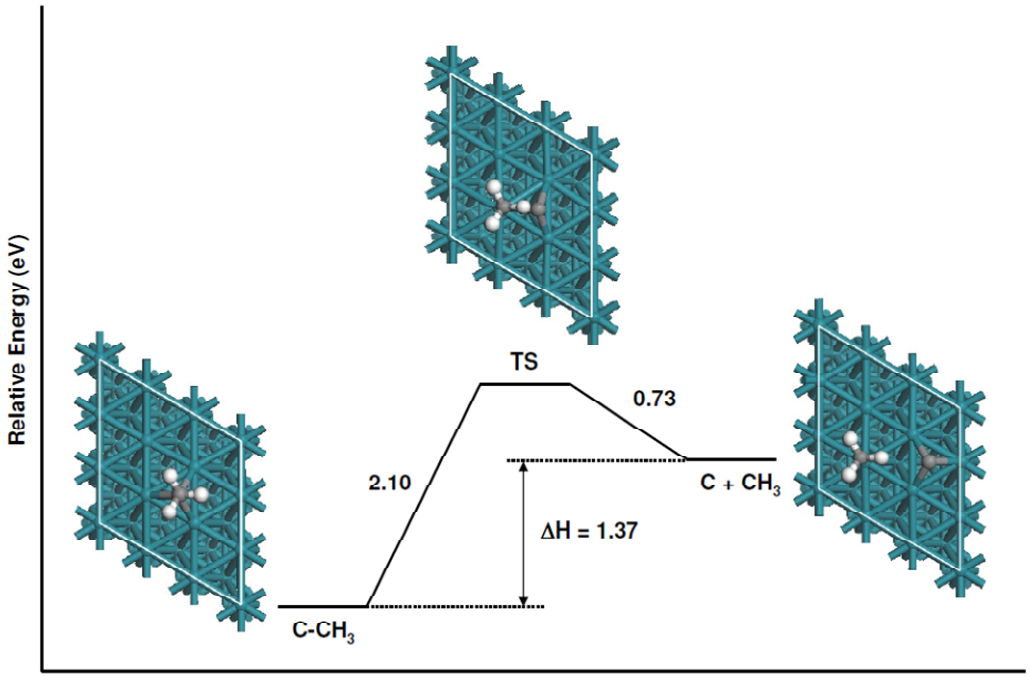


**Figure 3.7** Fragmentation of $CH_3CH$ to $CH_3$ and C via transition state TS

Vinylidene dehydrogenation to ethynyl species and also decomposition to methylene and carbon are the probable reaction occurring at the surface. C-C is bond breakage at this stage is not that feasible as high energy is required to break the double bond existing between carbon atoms and the activation energy for the reaction is found to be 2.41 eV. C-H activation is less for dehydrogenation to ethynyl species and is calculated as 2.12 eV.

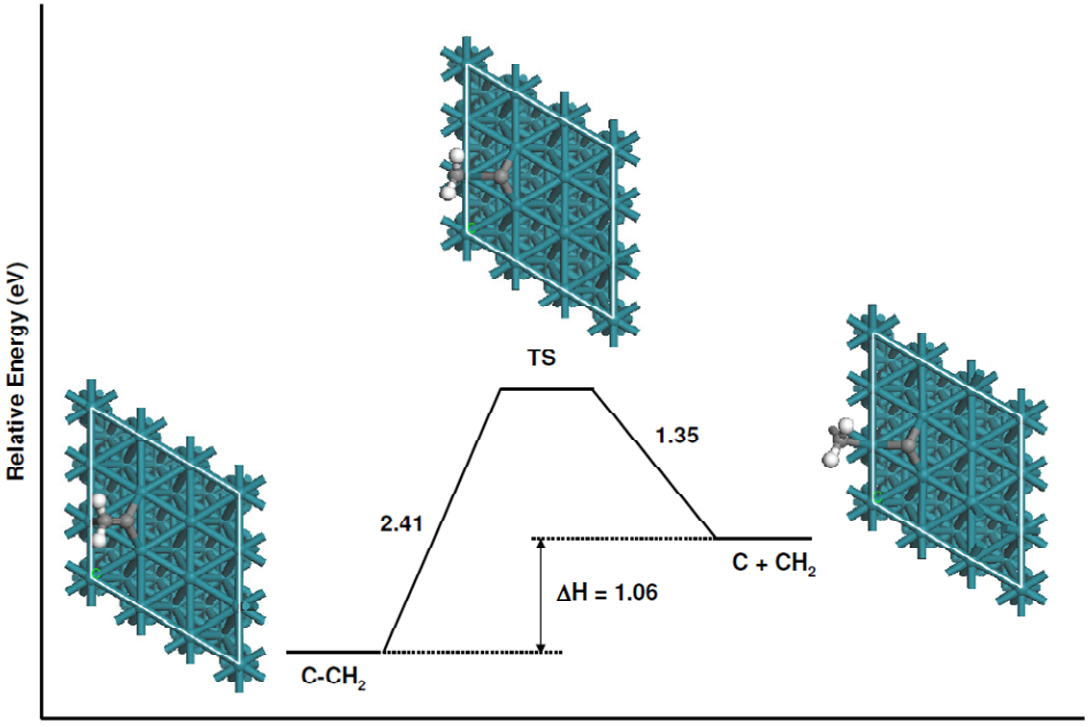


**Figure 3.8** Fragmentation of $CH_2CH$ to $CH_2$ and C via transition state TS

Ethynyl to methylidyne and H formation is facile as it is much less activated as compared with the competing reactions at this level. The activation energy of the reaction is found to be 1.35 eV and is slightly endothermic by 0.18 eV. Ethynyl to carbidic ethynylene(CC) is however not that favorable as the reaction is highly activated by 2.50 eV and is not likely at low temperature.

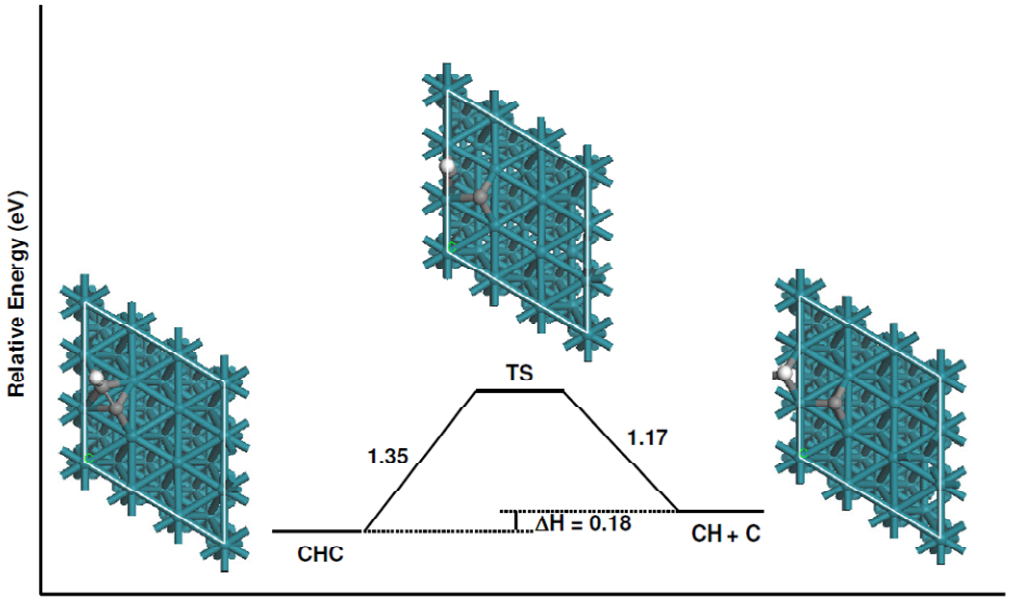


**Figure 3.9** Fragmentation of CCH to CH and C via transition state TS

carbidic ethynylene is very stable at the surface and C-C breakage occurs at very high temperature. So one of the main sources of C-atom on the surface can be clearly detected as the CHC fragmentation and thus ethynyl can be announced as the main source of atomic carbon produced at the surface from ethane dehydrogenation.

We summarize the fragmentation reaction of $C_2H_x$ in **Table 3.4**

| Fragmentation Reactions | Ea | ΔH |
|---|---|---|
| $CH_3CH_2 \rightarrow CH_3 + CH_2$ | 2.15 | 0.40 |
| $CH_3CH \rightarrow CH_3 + CH$ | 1.39 | -0.28 |
| $CH_2CH_2 \rightarrow CH_2 + CH_2$ | 2.20 | 0.70 |
| $CH_3C \rightarrow CH_3 + C$ | 2.10 | 0.73 |
| $CH_2CH \rightarrow CH_2 + CH$ | 1.90 | -0.05 |
| $CHCH \rightarrow CH + CH$ | 1.30 | -0.74 |
| $CH_2C \rightarrow CH_2 + C$ | 2.40 | 1.05 |
| $CHC \rightarrow CH + C$ | 1.35 | 1.16 |

**Table 3.4.** Activation energy and reaction energy in eV for fragmentation reactions of $C_2H_x$ species via C-C bond breakage.

At low temperatures ethane will dehydrogenate to form ethylene and at high temperatures ethylene will undergo further dehydrogenation to form further $C_2H_x$ species and fragmentation can occur with C-C bond cleavage leading to $CH_x$ and C in the surface.

## 3.5 Conclusions

Study of ethane dissociative adsorption provides a key model for catalysis involving molecules with C-C bonds. We have developed for the first time the complete pyrolytic $C_2$ chemistry for reaction on Rh(111) surface. Our studies strongly indicate that, at low coverages, the decomposition of ethane is initiated by C-H bond scission to form ethyl species. Two pathways are considered for ethylidyne formation from ethyl radical, where the first pathway proceeds via ethylidene ($CHCH_3$) and the alternate pathway proceeds via ethylene and vinyl ($CHCH_2$) species. Thus, $CH_2CH_2$ and $CH_3CH$ are easily formed on Rh(111) surface after ethane dissociative adsorption. The stable species $CH_3C$ is then rapidly formed on the surface from $CH_3CH$.

We computed the reaction energies for 24 elementary steps that may potentially be involved in the dehydrogenation, isomerization and fragmentation of ethane. Our calculations clearly indicate that the dehydrogenation of ethane to ethylidyne is kinetically and thermodynamically favorable. Besides, the C-C bond breakage by fragmentation of radicals before ethylidyne formation is energetically unfavorable. Ethylidyne is a stable species and decomposes at higher temperatures and it is interesting to observe that C-C bond disintegration prevails at this point and ethylidyne is thus precursor for formation of $CH_x$ radicals as indicated by present investigation. Thus in general, for larger hydrocarbons, during industrially important process like catalytic reforming, alkylidyne could be considered as prototype for C-C bond scission. Energetics of 1, 2 H-shift reactions are however not found favorable on Rh. Formation of CHC

is highly activated reaction but its dissociation to C and CH is found to be facile compared to other fragmentation reactions and is a potential source of C formed on Rh(111) surface according to our DFT calculations.

We have developed the $C_2$ chemistry of hydrocarbons on Rh(111) surface that can be combined with microkinetic simulation in the future and then comparison with experimental data can lead to understand the whole complex process better.

# Chapter 4

# Propane Dehydrogenation and Fragmentation on a Rh(111) Surface

## 4.1 Introduction

The production of hydrogen by catalytic partial oxidation reactions is a rapid process and is performed at short contact times. Methane partial oxidation has been studied extensively [75-80]. However, conversion of propane to synthesis gas by steam reforming or catalytic partial oxidation has been studied by only a few research groups. The experiments have been carried out using $Pt/Rh/CeO_2/Al_2O_3$ [81-84], $Pt/Pd/Al_2O_3$ [81, 82, 85-87] and $Ni/Al_2O_3$ [83] as catalysts. Steam reforming of propane is studied by Huff et al. and the sequence of the activity of metals is found to be: Rh > Pd > Pt [87]. Pd is found to behave similarly as Pt for the same reaction but there is limitation in using Pd catalyst as it is deactivated due to carbon deposition. It is also observed by experiments that the $O_2/C_3H_8$ ratio has a significant effect on conversion of propane and selectivity of hydrogen. The stoichiometric ratio of $O_2/C_3H_8$ leads to the formation of $CO_2$ whereas substoichiometric ratio leads to syngas formation.

Surprisingly, not much study has been devoted to the elucidation of the reaction mechanism of this industrially important catalytic system. Our aim is to perform a systematic study of the adsorption structures of $C_3H_x$ (x=2-7) species and to determine the energetics of the propane dehydrogenation reaction. We used periodic DFT calculations to determine the geometry, adsorption site preference and binding energy for all the species.

## 4.2 Adsorption of propane and $C_3H_x$ (x=2-7) Species

Propane is a closed-shell saturated hydrocarbon and thus shows very weak chemical interaction with the Rh slab and its adsorption is insensitive to the nature of the adsorption site. The potential energy surface of the adsorption is found to be quite flat. Propyl intermediates are involved in the dehydrogenation of propane and were also found to be an integral part of the thermal hydrogenation of propene, allyl, and metallacycloalkyl moieties to propane on Pt(111) [88,89].

Studies on propyne and propylene shows that both adsorb molecularly with the unsaturated bond nearly parallel to the surface on Pt(111) [90-93]. Over a range of surface temperatures, NEXAFS spectra is obtained [90,91] for propyne and propylene. Below 200 K, it is reported that propylene bond to the Pt(111) surface in a di-σ configuration. It is further observed that above 300 K, propylene undergoes dehydrogenation and form propylidyne in the absence of oxygen. $CH_3CHCH_2$ (propylene) adsorbs as di-σ bonded and π-bonded propylene on Rh(111) surface. On Pt(111), experimental studies [89] suggest that at the lowest coverages, a V-shape adsorption geometry of di-σ bonded species is obtained which is bonded to the metal through the central carbon atom. Above half saturation of the first layer, a rearrangement is observed towards a more horizontal C-C bond and a more vertical methyl group which is tilted away from the surface. We also obtain similar structure on Rh(111) even at 0.33 ML coverage, which is found as most stable propylene species and in this orientation, the molecules can pack better on the surface. The C-C bond length is found to be elongated by 0.14 Å than in gas phase indicating a saturated bond character in di- σ adsorption mode. Experiments shows that above saturation coverage of propylene, a second layer of weakly adsorbed π-bonded species grows and a clear transformation has been observed in the temperature range of about 230 and 270 K [94]. Propylene thus display another distinct adsorption geometry [89]

on Pt(111) where they interact weakly with the metal via π-bonding and is assumed as most likely species to be directly involved in the catalytic hydrogenation of propylene under atmospheric conditions. We also found a distinct π-bonded propylene formed on Rh(111) surface in consistence with experimental findings [95], where the species is bonded to two surface Rh atoms through its unsaturated bond.

$CH_3CH_2CH_2$ (1-propyl) and $CH_3CHCH_3$ (2-propyl) species adsorb preferably on the top site where the surface metal atom get attached to the C-atom from which dissociation of H atom takes place on Rh(111) surface.

$CH_3CCH_3$ (dimethyl carbene) is found to be stable as adsorbed on a bridged site where the middle C-atom is attached to the two adjacent surface Rh atoms.

In $CH_3CCH_2$ (2-propenyl), middle carbon is bridged between two Rh atoms and the terminal C binds to top site of a Rh atom. The geometry of all $C_3H_x$ is shown in Fig 4.1. Adsorption take place in a way that Rh(111) prefers sp3 bound $C_3H_x$ intermediates.

$CH_2CCH_2$ (allene) radical is adsorbed with the 2 terminal C-atoms bonded to the top site of Rh atoms and the middle C-atom is bridged between two other neighboring Rh atoms. Allene is found linear in the gas phase, however forms a flat V-shape on the surface upon adsorption.

Adsoprtion of Propyne resembles adsorption of acetylene on transition metal surface, with the π system nearly parallel to the surface [90]. Acetylene and propyne are stable up to 490 K. The methyl group in propyne is orientated up and away from the surface plane, allowing for dense packing on the Pt(111) surface [90]. A experimental study [96] reported that $CH_3CCH$ (propyne) also binds to the Rh surface with its unsaturated bond approximately parallel to the surface forming a 2x2 ordered pattern but no detailed information about the adsorption mode and adsorption site is available by experimental study. Our DFT calculation indicates that the propyne molecule adsorbs in hollow-parallel adsorption mode (di-σ/π) on Rh(111) surface.

$CH_2CCH$ (allyl) radical is stable in Rh(111) surface with $C_1$-$C_2$ double bond present in the molecule upon adsorption and both the C-atoms are sharing bridged site.

$CH_3CC$ (propynyl) binds clearly in a sp2 fashion similar to its on binding on Pt(111) surface [97] and it binds to the (111) surface in a η3η1 ($C_1$,$C_2$) adsorption mode. The $C_1$-$C_2$ bond is found to be 1.33 Å, which is close to double bond and $C_2$-$C_3$ bond is found to be 1.47Å, close to single bond.

$CH_2CC$ (propadienylidene) is adsorbed in η3 η2η1 ($C_1$, $C_2$, $C_3$) mode where $C_1$-$C_2$ bond is unsaturated with bond distance 1.33 Å .

In $CH_3CH_2CH$ (Propylidene) species, the terminal methylidyne C is attached to the surface and hence favours adsorption at a bridge site where the C atom binds to two neighbouring Rh atoms as shown in Fig 4.1**.**

$CH_3CH_2C$ (Propylidyne), just like ethylidyne binds the surface through carbon atom having no hydrogen atom present and prefers to bind to 3-fold hollow sites. There is also experimental evidence for the structure and binding preference of propylidyne on noble metals and our study is in line with the structure obtained [88]. However propylidyne is found to prefer fcc site in Pt(111) but in Rh(111), we observe a slight preference towards hcp site.

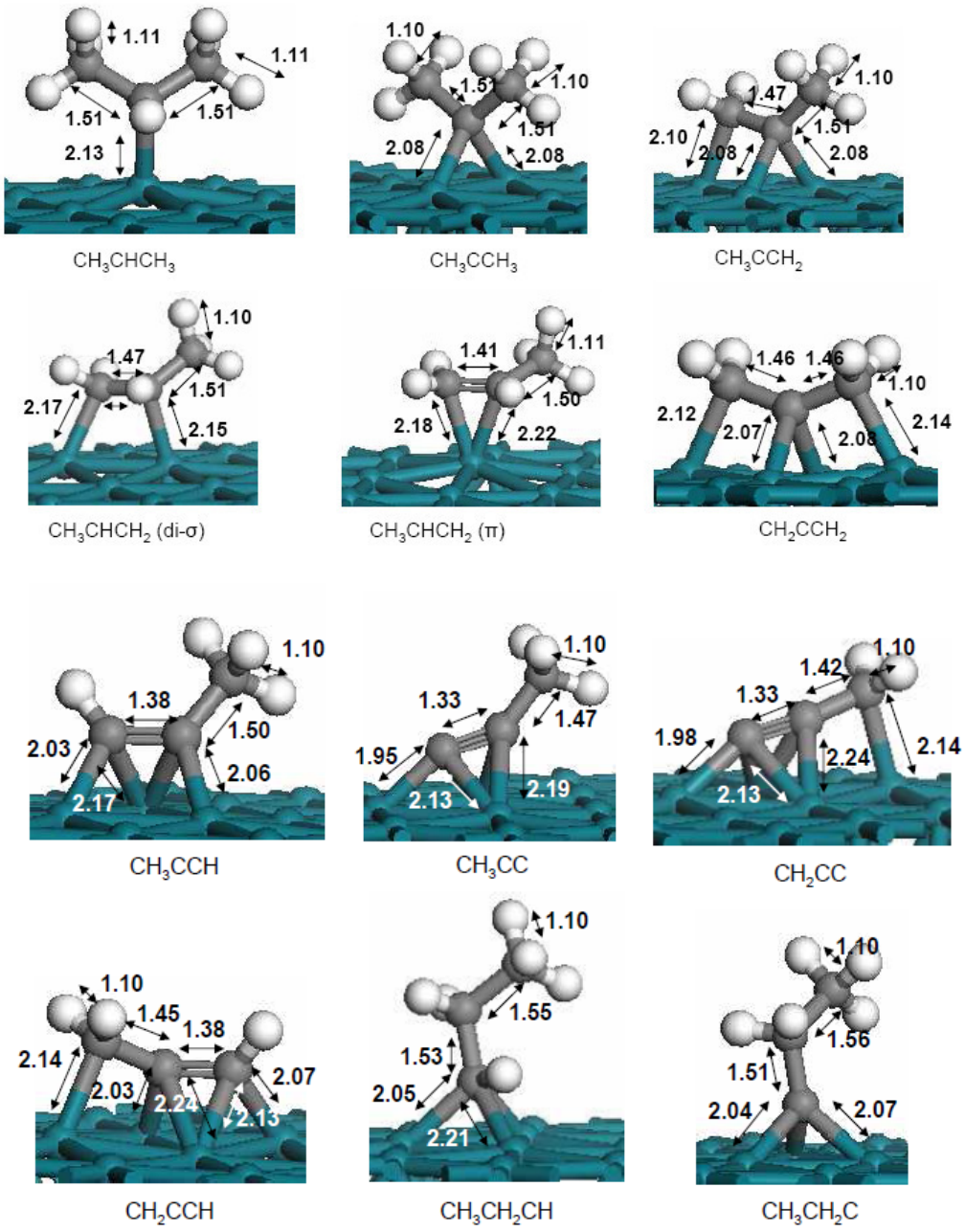


**Fig 4.1. Adsorption geometry of $C_3H_x$ radicals**

## 4.3 Reaction Pathways and Activation Barriers

Reaction pathways are given in scheme 4.1, where in this chapter we only consider important elementary steps to discuss in detail.

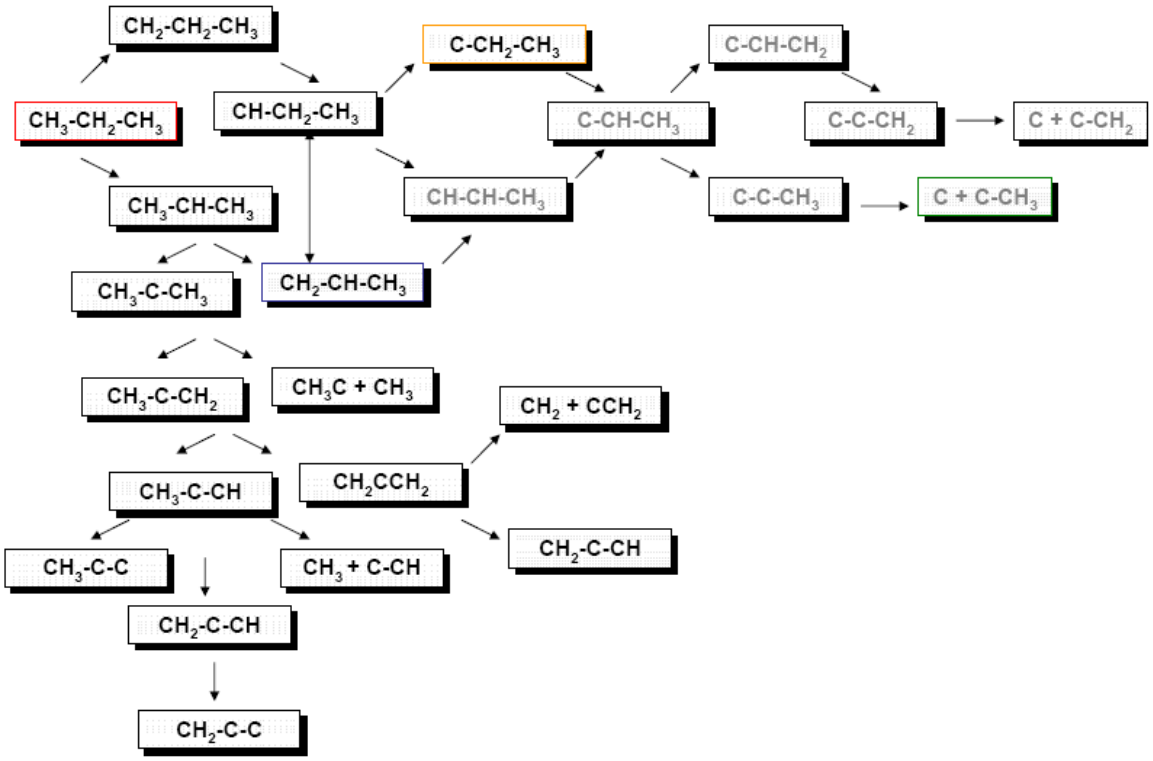


**Scheme 4.1.** Plausible reaction scheme propane decomposition

### 4.3.1. Propane to 1-propyl and 2-propyl formation

Dissociative adsorption of propane is a crucial step as in most catalytic reactions involving hydrocarbons, the activation of C–H bonds in alkanes to yield surface alkyl groups is believed to be the rate limiting step.

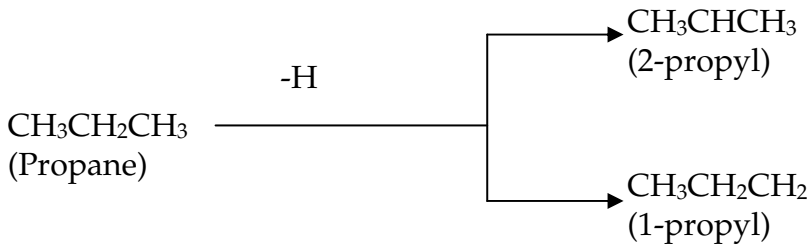


**Scheme 4.2** Propane dissociative adsorption

The breaking of a propane C-H bond can occur in the terminal methyl (-$CH_3$) or the middle methylene (-$CH_2$) group of propane, and the corresponding products are 1-propyl or 2-propyl species on the Rh(111) surface. From thermodynamics, it is known that the C-H bond energy in the methyl group is stronger than that in the methylene group (420 kJ/mol and 401 kJ/mol respectively). The trapping-mediated dissociative chemisorption of three isotopes of propane $C_3H_8$, $CH_3CD_2CH_3$, and $C_3D_8$ has been investigated by Weinberg et al on the Pt(110)-(1 x 2) surface, the probabilities of primary and secondary C-H bond cleavage for alkane activation on a surface were evaluated [98]. The activation energy for primary C-H bond cleavage was 425 calories per mole greater than that of secondary C-H bond cleavage, and the two true activation energies that embody the single measured activation energy were determined for each of the three isotopes. Secondary C-H bond cleavage is also preferred on entropic grounds, and the magnitude of the effect was quantified.

We have studied dissociative adsorption of propane on the Rh(111) surface and the energy diagram for the formation 2-propyl species from dehydrogenation of propane is described in Fig 4.2.

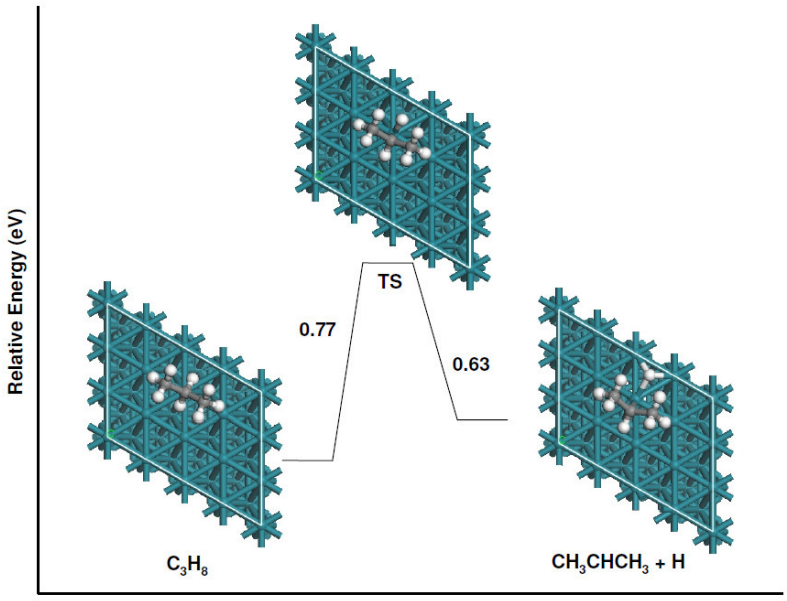


**Fig 4.2.** Propane to 2-propyl formation

Propane from gas phase approaches the surface and undergoes dissociative adsorption. In the transition state the C-Rh bond formation starts and the middle C-atom of propane is at a distance of 2.31 Å from the top site of Rh atom and both the C-C single bond is measures as 1.51 Å. H-atom disintegrates at the same top site of Rh, which is shared by C-atom of propane and then stabilizes by migrating to the next fcc site.

We investigate the first step for C-H activation for propane and it is found that 2-propyl species formation is more favored on Rh(111) surface, for which the structures and energy diagram are described in **Fig 4.2**. The dehydrogenation of propane on Rh(111) proceeds to propylene mainly through 2-propyl intermediate.

### 4.3.2. 2-propyl Dehydrogenation Reactions

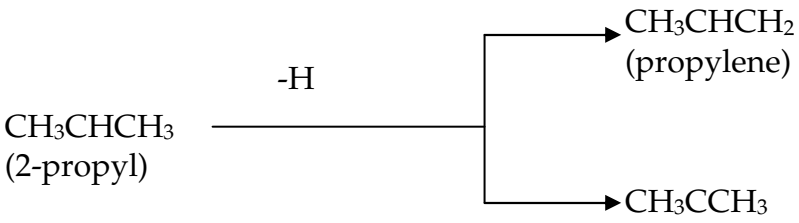


**Scheme 4.3** 2-propyl dehydrogenation to $CH_3CHCH_2$ or $CH_3CCH_3$

The formation of propylene via $\beta$-hydride elimination was identified by isotopic labeling TPD experiments, and directly about 200 K by RAIRS [99]. Comparing the relative rates of $\beta$-hydride and reductive elimination for both 1-propyl and 2-propyl intermediates on Pt(111) surface, it is clear that the 2-propyl intermediate favors propylene production . Studies on propane oxidation however shows that propylene is the primary oxidation product of propane at low oxygen conversions but it is not the main intermediate product at high conversions [100].

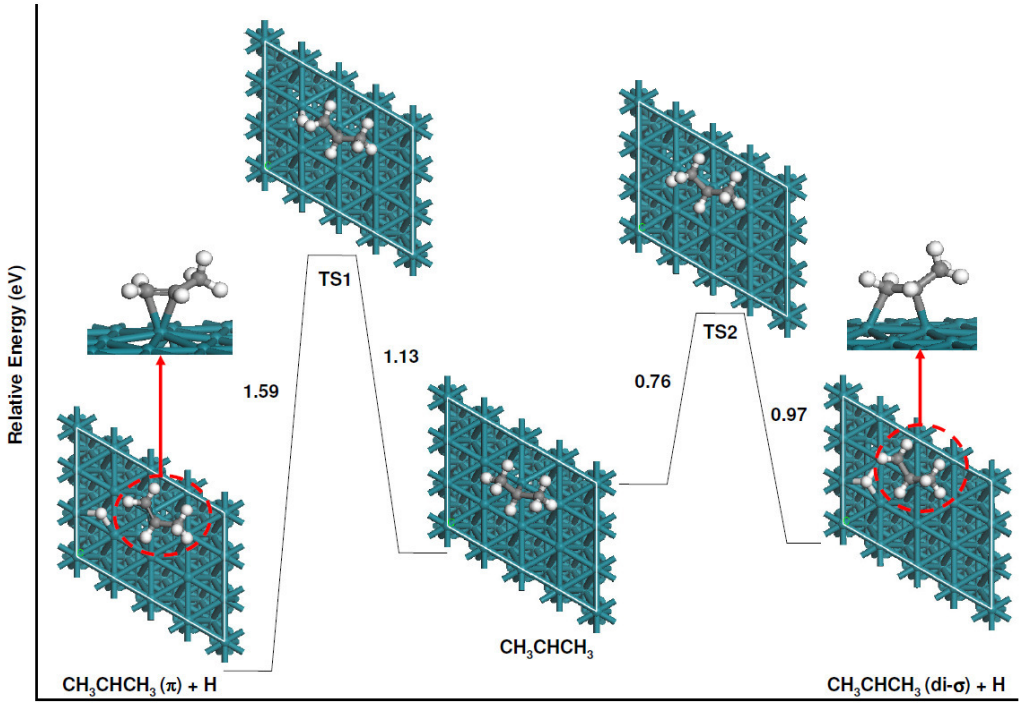


**Fig 4.3** 2-propyl to π-bonded propylene and di-σ bonded propylene

2-propyl species is attached to the surface through the middle carbon on the top site of Rh(111) surface. This species is an important intermediate species formed during dehydrogenation of propane and found to be the dominant source of propylene at the surface according to our calculations. In the transition state for the formation of propylene, $C_2$-Rh distance in TS1 and TS2 is 2.20 and 2.13 Å respectively. Di-σ bonded propylene formation reaction from 2-propyl is found to be activated by 0.76 eV. According to our calculation for this reaction, the reaction enthalpy is -0.21 eV whereas in Pt(111) [99] the energy of reaction is higher and is reported as -0.32 eV. We have found the activation energy for the formation of π-bonded propylene is 1.13 eV and the energy of reaction is -0.45 eV.

Reactions of propylene in di-σ configuration are given in Scheme 4.4.

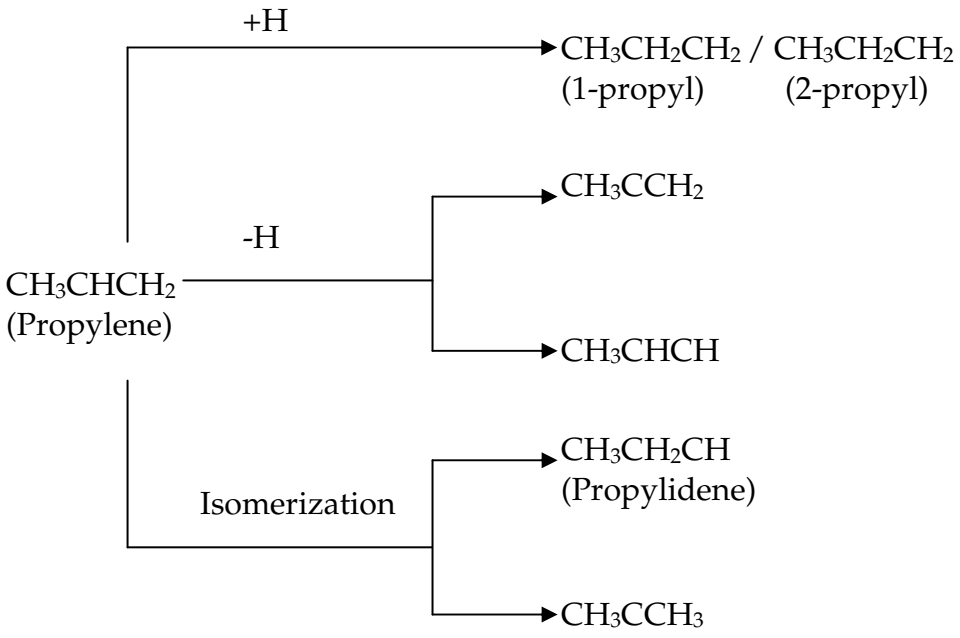


**Scheme 4.4** Dehydrogenation and isomerization reactions of propylene

Many studies has been carried out for the route to propylidyne from propylene. Di-σ propylene can undergo dehydrogenation to form $CH_3CHCH$ or $CH_3CCH_2$. Propylene can also undergo isomerization to form propylidene species or $CH_3CCH_3$. Propylene can also hydrogenate in the surface to generate 1-propyl species, from which also propylidyne can be formed on subsequent dehydrogenation. Pathway to propylidyne is also obtained from 1,2 hydrogen shift of chemisorbed propylene to propylidene followed by dehydrogenation. The most important reaction from propylene is found to be the formation of propylidyne, which is found stable species at the surface. TDS [101] and secondary ion mass spectrometry results [102] indicate that propylidyne is formed from propylene at the same temperature of 200K as ethylene forms ethylidyne on Pt(111) surface. On both Pt(111) and R(111) surface, propylidyne forms (2x2) LEED patters [103]. According to our DFT calculation, the formation of propylidyne from propylene occurs via its first isomerization to propylidene and then subsequent dehydrogenation leads to the formation of propylidyne species.

Apart from the formation of propylene, another important reaction of 2-propyl species on Rh surface to the formation dimethyl carbene is investigated. The transition state structure and energy diagram for the reaction is described in Fig 4.4.

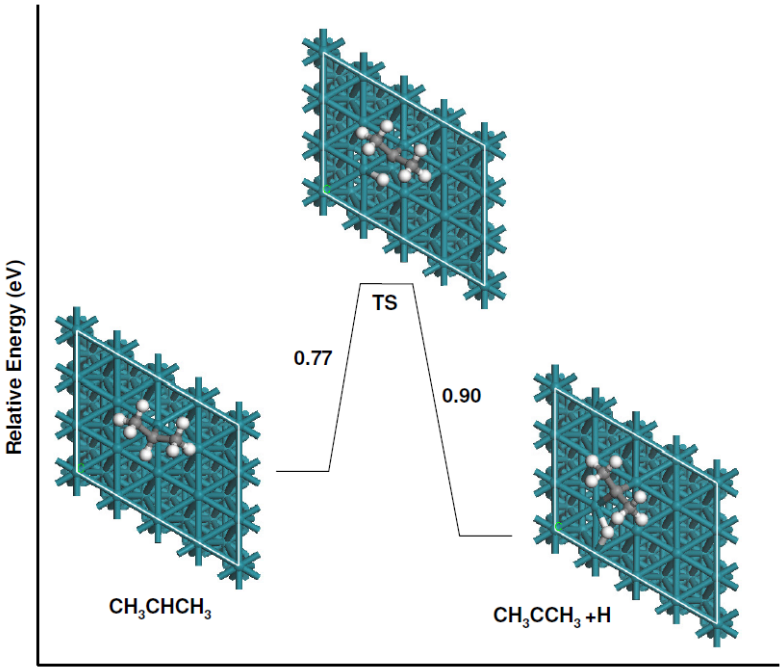


**Fig 4.4** 2-propyl formation to $CH_3CCH_3$ species

Dehydrogenation from the middle C-atom of 2-propyl species leads to the formation of $CH_3CCH_3$ species, which is also identified as intermediate species on the surface. This reaction is activated by 0.77 eV and the reaction enthalpy is -0.13 eV. According to our investigation, the formation of di-σ bonded propylene and dimethyl carbene species are almost equally kinetically favorable on Rh(111) surface at a given temperature.

### 4.3.3. Reaction of $CH_3CCH_3$ and Propyne Formation

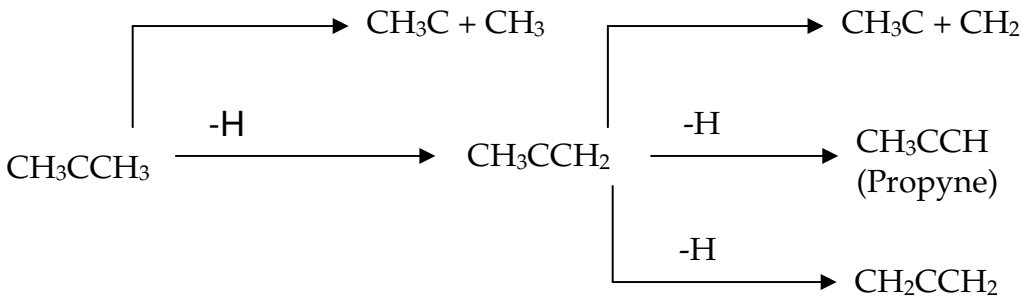


**Scheme 4.5** Dehydrogenation and fragmentation reaction of $CH_3CCH_3$

$CH_3CCH_3$ radical formed on the surface is symmetric and its adsorption mode has resemblance to adsorption of $CH_2$ molecule with 2 H-atoms replaced by $–CH_3$ groups, however due to repulsion between two comparatively bulky methyl groups, the molecule is a bit flat than $CH_2$ in the surface. $CH_3CCH_3$ undergo dehydrogenation which leads to the formation $CH_3CCH_2$ as a precursor to the formation of adsorbed propyne in the Rh(111) surface. The dehydrogenation to $CH_3CCH_3$ takes place by activation of one H of the two methyl group and then in the transition state the H-atom stay over top of a Rh atom and then subsequently diffuses to the neighboring fcc site. The dehydrogenation is activated by 0.63 eV and the reaction is found to be almost thermoneutral. However the activation energy for fragmentation of $CH_3CC$ is much more than double of that for dehydrogenation reaction and is found to be 1.57 eV. Fragmentation is observed to be exothermic by -0.16 eV leading to the formation of ethylidyne and methyl radical in the surface.

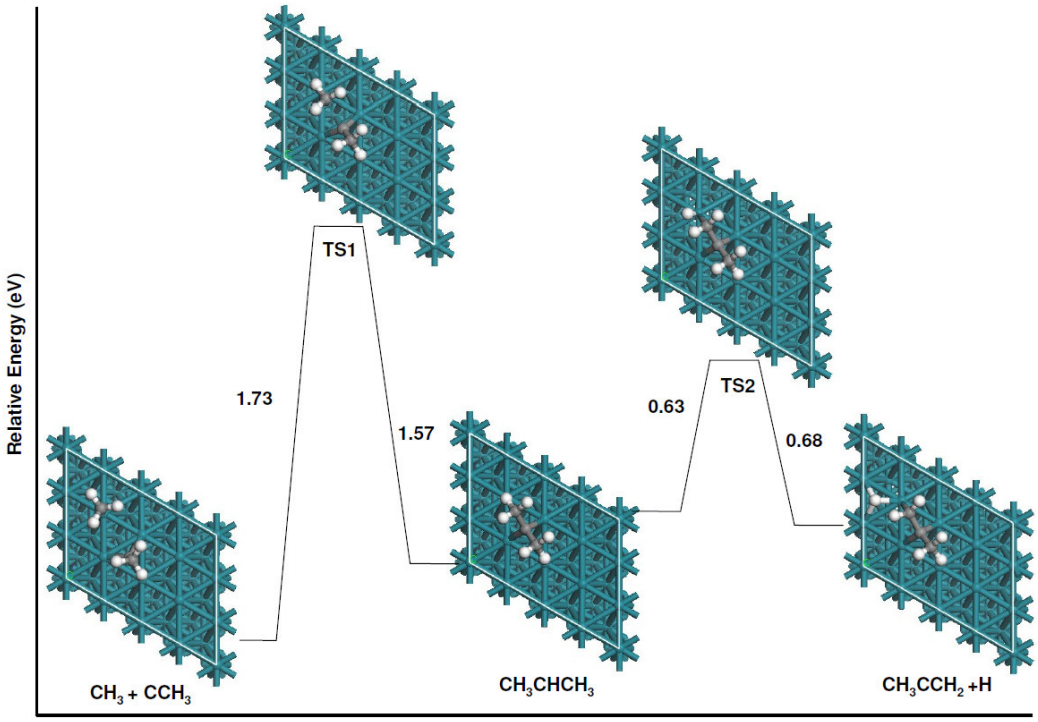


**Fig 4.5.** $CH_3CCH_3$ to $CH_3CCH_2$ and $CH_3$, $CCH_3$

Propyne is readily formed in Rh(111) surface from the dehydrogenation of $CH_3CCH_2$ and the reaction is activated by 0.55 eV and energy of reaction is found to be -0.10 eV. The other competing reaction is the formation of $CH_2CCH_2$. The sequential dehydrogenation of $CH_3CCH_2$ to propyne and $CH_2CCH_2$ over Rh is shown in Fig 4.5.

Route to propyne from propylene is reported on Pt(111) [97] surface through the 2-propenyl intermediate. The initial dehydrogenation of propyne to 2-propenyl species is found almost thermoneutral with energy of reaction -0.02 eV and further dehydrogenation of 2-propenyl to propyne is shown exothermic with reaction enthalpy -0.17 eV, which is slightly higher by 0.7 eV than we have observed in Rh(111) surface.

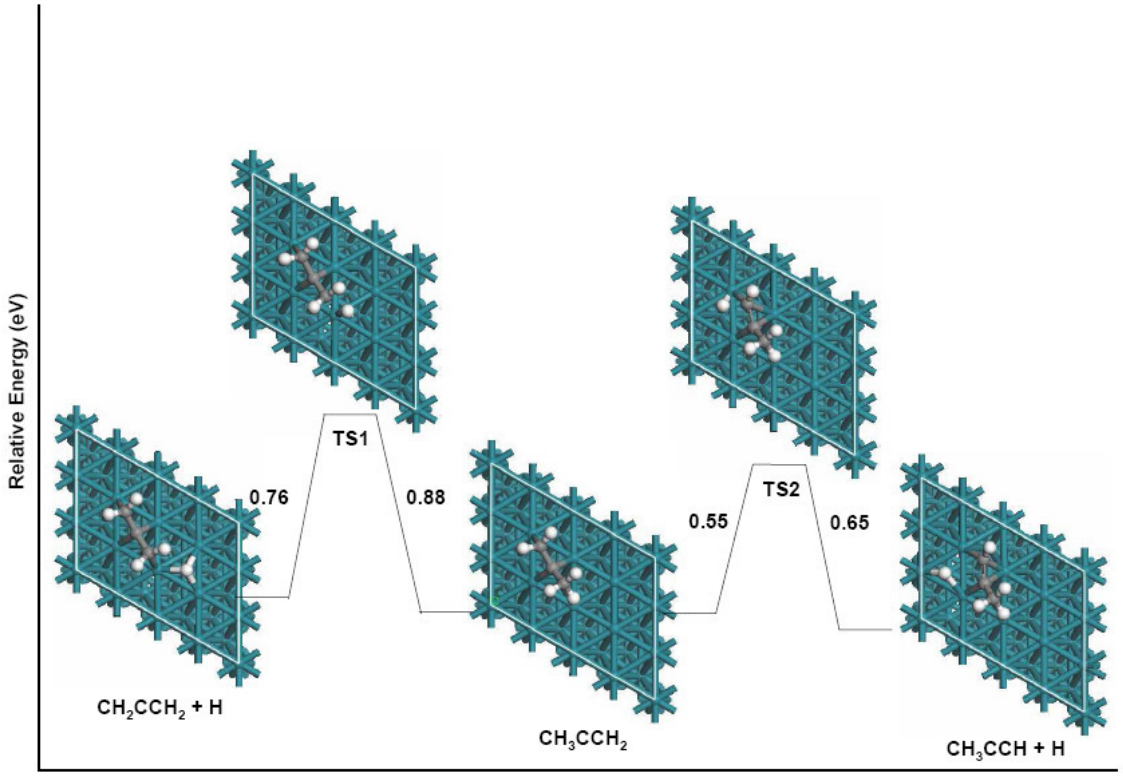


**Fig 4.6.** $CH_3CCH_2$ to $CH_3CCH$ (Propyne) and $CH_2CCH_2$

In the transition state for propyne formation, a hydrogen is given out at the top site of a Rh atom by one of the terminal carbon $C^1$ of 2-propenyl species at a distance of 1.44 Å and $C^1$-$C^2$ bond distance is found 1.40 Å, which is a double bond and the TS species remain bonded to the surface through $C^1$ and $C^2$ atoms. The $CH_2CCH_2$ species is also formed by dehydrogenation of 2-propenyl which generates propyne on surface. In the transition state the H is detached from the methyl group present in 2-propenyl at a distance of 1.64 Å and the TS is bonded to the surface through $C^2$ and $C^3$, where $C^2$-$C^3$ forms a single bond of 1.48 Å.

The $CH_2CCH_2$ species which is formed instantaneously then get readily converted to $CH_2CCH$. The activation energy for the reaction is 0.40 eV and energy of reaction is found to be -0.16 eV. The reactant, product, TS structures and energy diagram for the formation of allyl species is shown in Fig 4.7.

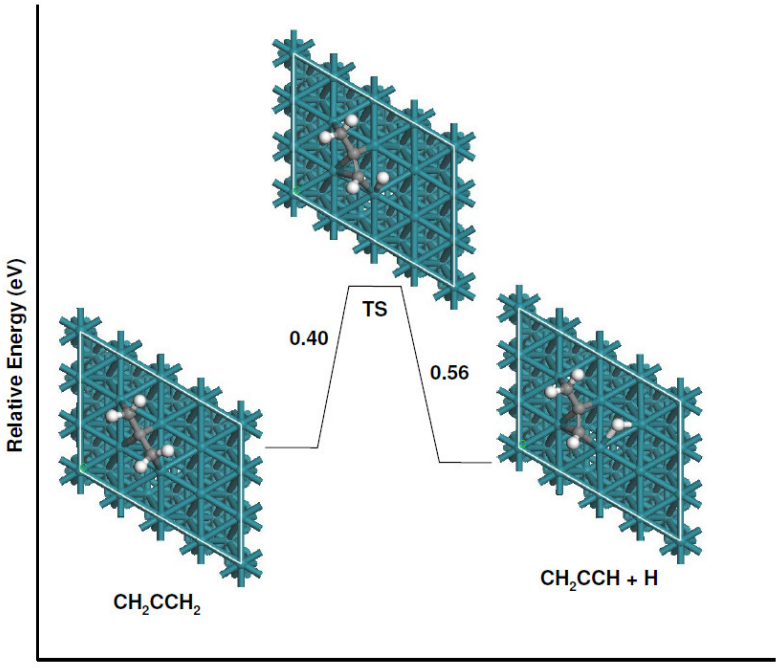


**Fig 4.7.** $CH_2CCH_2$ to $CH_2CCH$ and H

In the transition state during dehydrogenation of $CH_2CCH_2$, the H-atom is abstracted from one of the equivalent terminal methylene group present in the reactant molecule. The $C^1$-$C^2$ and $C^2$-$C^3$ bond shortens at TS to 1.40 Å and 1.45 Å respectively than in reactant molecule for which the both C-C bond distance is 1.48 Å.

The dehydrogenation reactions of $CH_3CCH_2$ is discussed, now additionally it also undergoes C-C bond breakage reaction along the two C-C bonds leading to the formation of $CH_2$, and $CCH_3$ on one hand and $CH_3$ and $CCH_2$ on the other hand. There is a possibility to get the stable $CCH_3$ molecule from the fragmentation reaction of $C_3H_x$ molecules like from $CH_3CCH_2$ species. However, the fragmentation reactions of $C_3H_x$ are found to have high activation energy and thus are only possible at high temperatures.

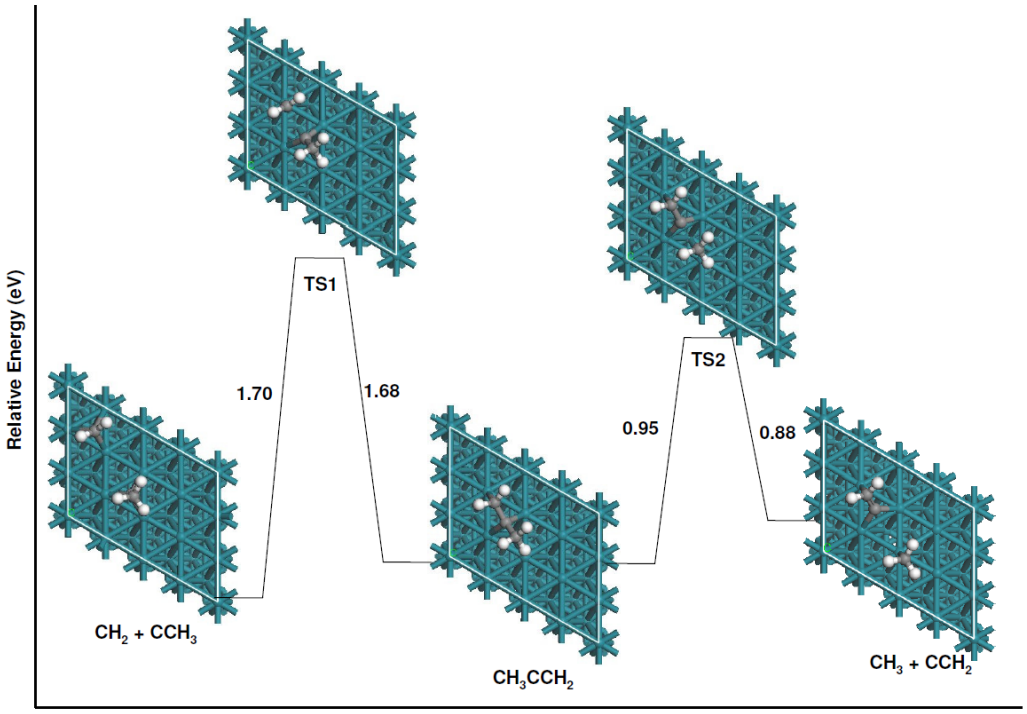


**Fig 4.8** $CH_3CCH_2$ to $CH_2$, $CCH_3$ and $CH_3$, $CCH_2$

The reactant, product and transition state structures for the fragmentation of 2-propenyl species are given in Fig 4.8. The formation of ethylidyne and methylene species by fragmentation is uphill by 0.73 eV than the formation of methyl and vinylidene ($CCH_2$) as fragmentation products on Rh(111) surface. In TS1 the $C^1$-$C^2$ bond is broken and set apart by 2.39 Å whereas in TS2 the $C^2$-$C^3$ bond undergoes cleavage and separated by 2.32 Å to produce the corresponding products.

### 4.3.4 Reactions of Propyne

Possibility of propyne activation on Rh(111) surface is demonstrated in scheme 4.6.

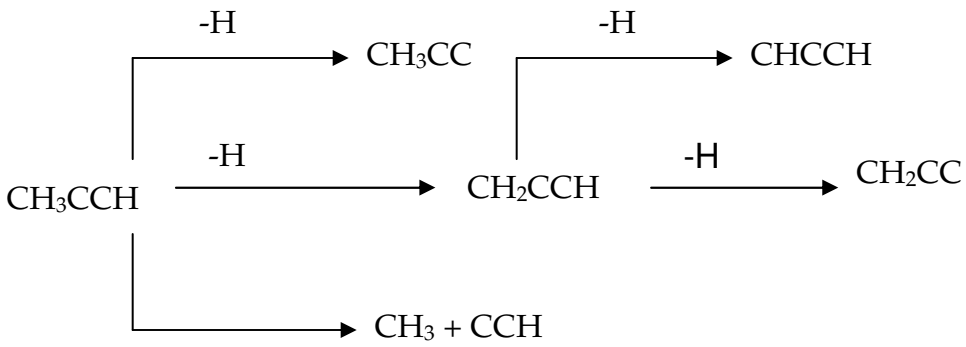


**Scheme 4.6** Dehydrogenation and fragmentation reactions of propyne ($CH_3CCH$)

Experimental study of propyne adsorption and decomposition has been reported on Pt(111) and Sn/Pt(111) surface alloys [104] and dehydrogenation is the major reaction pathway found on the Pt(111) surface. Propyne formed on Rh(111) surface is found to be strongly adsorbed with adsorption energy -2.17 eV and the adsorbed propane at the surface is has very different structural arrangement than the gas phase linear Propyne molecule. It bonds to the surface through the unsaturated C-C bond. Its dehydrogenation from two terminal C-atom, $C^1$ and $C^3$, leads to the formation of Propynyl species ($CH_3CC$) and $CH_2CCH$ respectively. For the conversion to propynyl, the H atom migrates through a hcp site at the transition state to the fcc site whereas for the conversion to $CH_2CCH$, the hydrogen atom is activated towards the top Rh center subsequently migrating to a neighboring hcp site. The activation energy for the formation of $CH_3CC$ is 1.42 eV. The reaction is observed exothermic with reaction enthalpy -0.45 eV, which is much higher than the formation of $CH_2CCH$ for which the energy of reaction is -0.08 eV. Fragmentation is not found favorable in propyne as the reaction has very high activation barrier of 2.39 eV. The energy profile of the dehydrogenation reactions of propyne are shown in Fig. 4.9 and of allyl species is given in Fig 4.10.

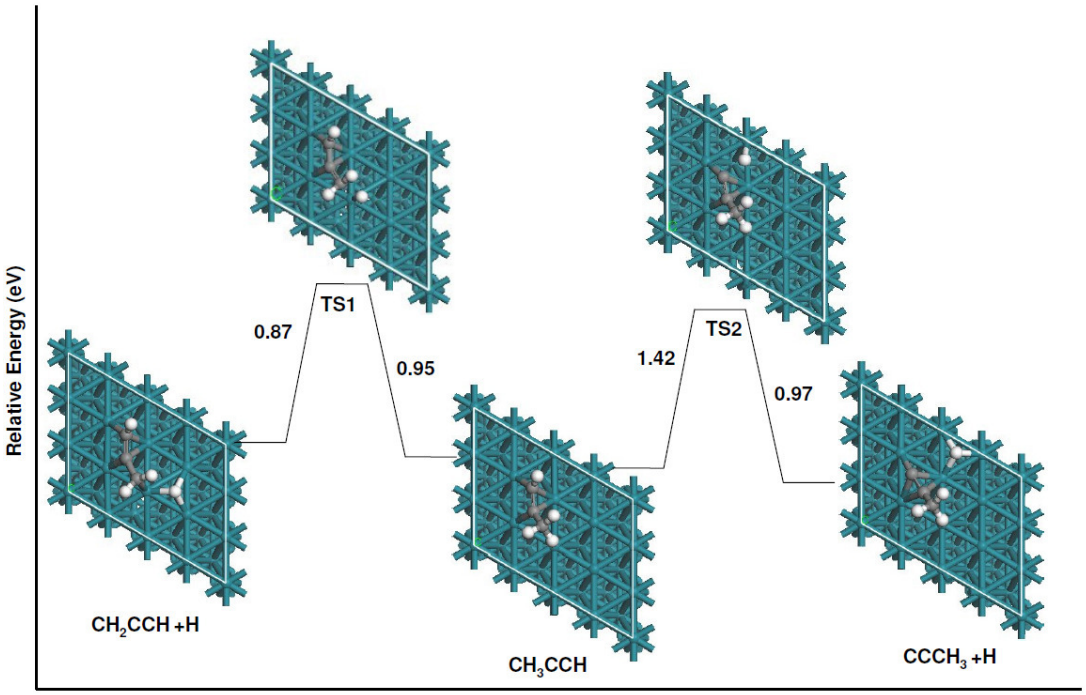


**Fig 4.9.** $CH_3CCH$ to $CH_2CCH$ and $CCCH_3$, H

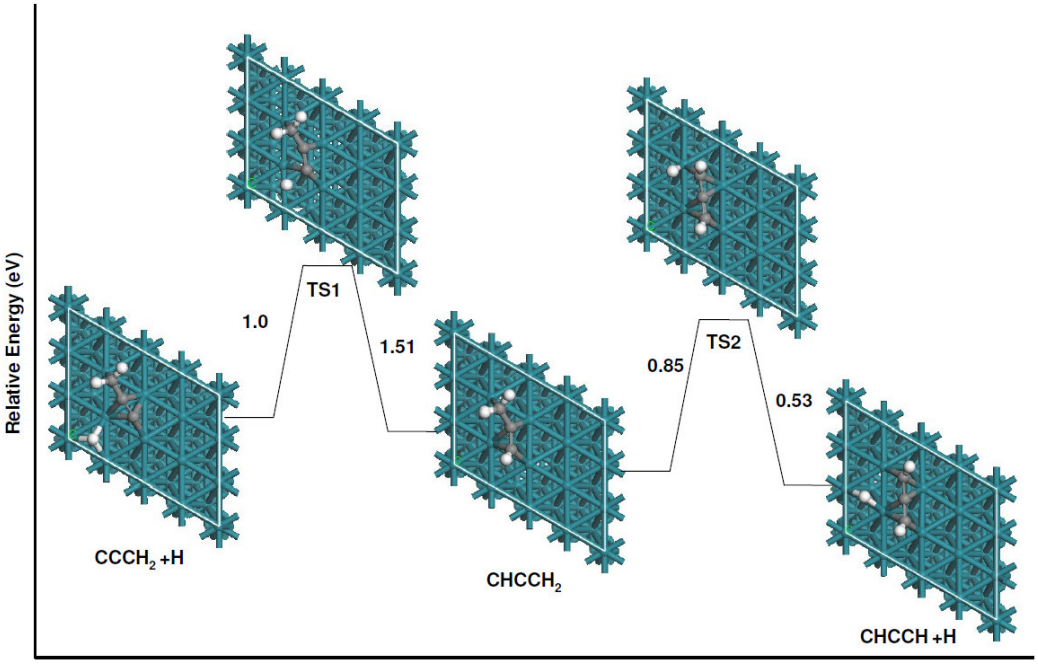


**Fig 4.10** $CHCCH_2$ to $CCCH_2$, H and CHCCH, H

The dehydrogenation of $CH_2CCH$ leads to the formation of $CH_2CC$ and CHCCH. $CH_2CC$ formation reaction has energy of activation 1.51 Å and the reaction is highly exothermic. The activation energy for CHCCH formation is found to be 0.85 eV and the reaction energy is -0.32 eV. $CH_2CCH$ thus can be traced as one of the source for the stable $CH_2CC$ species on the Rh surface. However at low temperature, dehydrogenation of allyl species leads to the kinetically favorable CHCCH species over the catalyst surface.

## 4.4 Conclusions

We present a comprehensive survey of the mechanism of dehydrogenation reaction of propane over various sites on the Rh(111) surface by using periodic DFT methods. A number of reaction mechanisms have been explored for the initial C-H bond activation and 2-propyl species formation is found to be dominant in Rh(111) surface.

Propylene is observed to be rapidly formed on the catalyst surface from propane dehydrogenation. Two stable configurations of propylene is observed where di-σ bonded propylene is comparatively more stable than the π-bonded propylene. We found the geometrical parameters and preferred adsorption sites for other $C_3H_x$ (x=2-7) radicals like 1-propyl, 2-propyl, propylene, dimethyl carbene, allene, allyl, propynyl, proadienylidene, propylidene and propylidyne at a surface coverage corresponding to a 4x3 unit cell. It is found that the $C_3H_x$ (x=2-7) fragment on Rh(111) surface preferentially occupies a site that completes the carbon tetravalency. Propylidyne is observed to be the most stable surface species on Rh(111) surface and our findings are consistent with the experimental evidence. We also identify alternate routes to propyne formation. It is observed that other than propylene, dimethyl carbene also leads to the formation propyne by successive dehydrogenation. Both the reaction however proceeds through 2-propenyl intermediate.

The important dehydrogenation and fragmentation reactions are considered in the Rh surface corresponding to the reactions occurring after propane dissociative adsorption and we thus elucidate the reaction mechanism on the catalytic surface of Rh.

# Chapter 5

# Hydrocarbon Decomposition in Presence of Oxygen

## 5.1 Introduction

One industrially useful application involving alkyl radicals and oxygen is the partial oxidation of hydrocarbons. Since saturated hydrocarbons are stable molecules, a lot of energy is needed to break one of its C–H bonds. Also, hydrocarbon fragments formed from hydrocarbon are so reactive that reactions most often proceed to complete combustion. Reacting alkyl radicals with oxygen directly via heterogeneous catalysis would also make the formation of alcohols and aldehydes. Therefore, it is essential to study the co-adsorption of alkyl radicals and oxygen on transition metal surfaces and the possible reaction pathways have to be developed since it is essential to obtain detailed information for the crucial elementary steps to either block or enhance particular steps to drive the reaction in the desired direction.

Alkyl radicals show different behavior in surface and needed to be explained on the basis of a detailed study. An interesting feature of methyl radical adsorption observed on transition metal surfaces is the presence of a weakened symmetric C–H stretch mode, which sometimes become shifted by hundreds of $cm^{-1}$ and was detected experimentally on Rh [105], Ni [106] and Cu [107–109] surfaces. Softened C–H modes have also been seen for other hydrocarbons and fragments on transition metals [110]. To understand the mechanism for this weakened C–H stretch, there has been much interest in exploring the study as it has possible relevance to dehydrogenation. Various investigations of mode-softening have

yielded a range of explanations, some contradicting others. The industrial importance and the unresolved fundamental issues make the methyl–surface interaction an excellent example of where first principles calculations can provide insight. We used first principles method and carried out a series of calculations to investigate the adsorption geometry and energy of methyl and other stable alkyl radicals generated from hydrocarbons. The development of modern theoretical surface sciences provides an opportunity to investigate surfaces and adsorbate structures on the atomic scale with useful applications in industrial technologies, which is also useful to improve our understanding of surface chemistry process as catalysis. In this chapter we mainly focus on the geometry and reactions of alkyl radicals coadsorbed with oxygen to learn more about the effect of this electronegative coadsorbate relevant to partial oxidation.

## 5.2 Mechanistic Pathways for Reaction of $CH_x$ and Oxygen

The adsorption of $CH_4$ on (111) facets of noble metals is highly activated because of the stability of its closed-shell and covalent structure and hence the sticking probability of $CH_4$ is extremely small on any solid surface system. So, in general, one of the rate-limiting steps in catalytic reactions involving methane is the C-H bond activation [111].

The chemisorption of methane on transition metal surfaces has been extensively studied experimentally [112-115 and references therein] and theoretically [116-120]. Many experimental investigations were carried out using molecular beam techniques [114] particularly on Ni, Pt and Pd. The activation barrier for dissociative adsorption of methane on Pt(111) has been studied in dynamical calculations based on thermally assisted tunneling. Dissociative chemisorption of $CH_x$(x=0-3) from methane has been studied with molecular beam techniques [121] and first principle calculations [122, 123].

Molecular beam surface scattering studies reveal that the dissociation probability of $CH_4$ is much smaller for the oxygen precovered surface than for the clean

surface [20]. It is also found that oxygen poisons the C-H activation and the poisoning is due to the fact that oxygen sterically blocks the active surface sites for dissociative chemisorption of $CH_4$ and forbids the dissociation electronically. The $CH_4$ activation mechanism is however expected to be the same for the clean and oxygen covered Pt( 111) surfaces [124].

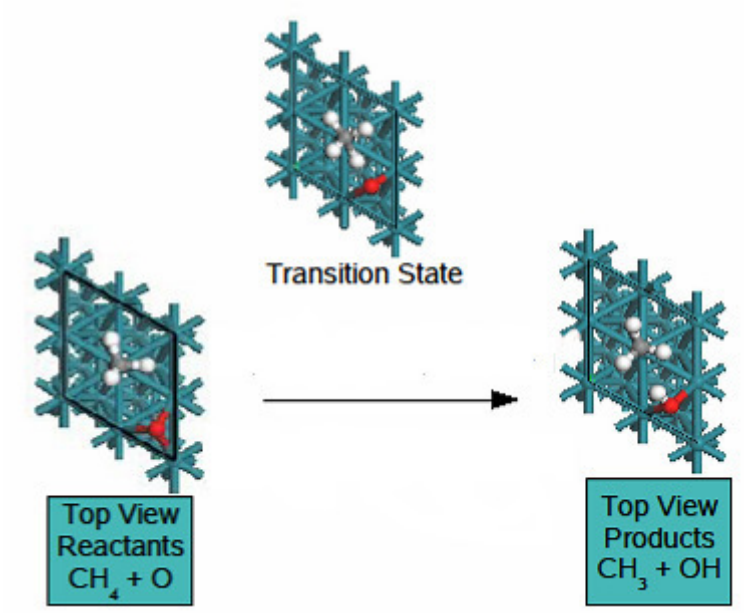


**Fig 5.1.** H-abstraction from $CH_4$ by a coadsorbed oxygen

Methane is studied in the presence of co-adsorbed oxygen and hydrogen abstraction by oxygen atom is studied. The reaction leads to the formation of methyl and hydroxyl species. The activation energy for the reaction is found to be 1.17 eV and energy of reaction is found to be 0.24 eV. The C-H bond is stretched to 1.56 Å from 1.11 Å in the transition state. The reaction is however found to be much more activated than in the absence of O-atom which is activated by 0.72 eV and hence it is unlikely that the first abstraction of methane does not occur readily by coadsobed oxygen at low temperature. Even though activation energy of the reaction in presence of oxygen is slightly higher than the

decomposition activation energy, these reactions are an alternative pathway to surface carbon formation, especially at high oxygen coverages.

$C_1$ hydrocarbon fragments on noble metals have been investigated by several groups [125-133]. It is found that for adsorption of $CH_x$ fragment on surface it appears to be a general trend that Rh(111) prefers $sp^3$ bound intermediates.

Understanding the bonding of oxygen to transition metal surface is also important to elucidate the role of oxygen in many catalytic reactions. Experiments using XPS, UPS and NEXAFS have been carried out study the bonding of atomic oxygen to Pt(111) surface [134] and the bonding is explained through the interaction of 2pxy orbitals of oxygen with the 5d orbitals of Pt metal. The chemistry of oxygen reactions on surfaces like Ag(110) are presented in terms of acid-base chemistry where oxygen abstracts a proton from the reactant molecule and assumed to act as a Brönsted base. This is often observed to be applicable in the case of Pt(111) surfaces where OH is formed on the surface as stable species and oxygen is believed to promote dehydrogenation reactions. It is however found that the behavior of oxygen is interestingly different in different transition metals. Studies on methanol oxidation over polycrystalline Pt and Rh reveal that the oxygen on Pt enhances catalytic activity whereas oxygen passivates the Rh Surface [135]. This behavior is however attributed to the stability of hydroxyl species on Pt than on Rh. The reactivity of oxygen with hydrogen and hydrocarbons is also strikingly different on Pt(111) and Rh(111) [136] as it is observed that oxygen inhibits C-H bond breaking on Rh(111) [137] whereas it promotes dehydrogenation of cyclohexane on Pt(111) surface [138]. Oxygen is strongly found to be strongly bound to Rh than Pt and this may de due to the degree of the filling of the d-band [139]. It is established that when an adsorbate that when an adsorbate having localized orbitals interacts with a metal which has a band of delocalized states like sp band of a metal, the localized orbitals are broadened into resonances [140]. Also, localized d states on the metal interact with the adsorbate to give bonding and

antibonding states. When the orbitals are half-filled, the bonding interactions are strong. The d bands of both Rh and Pt metals are though greater than half-filled, the Pt d band is more filled than Rh, which leads to greater antibonding interactions with the 2p orbital of oxygen. For the sp band, Rh has a stronger interaction with oxygen.

In Rh(111) surface, our calculations indicate that atomic oxygen prefer 3-fold hollow sites as compared to top or bridged sites, which in accordance with LEED studies [140].

After dissociative adsorption of methane, subsequent dehydrogenation takes place and the last dehydrogenation step is found to be crucial for many important industrial reactions. Reactions of methylidyne (CH) are also believed to be one of the rate determining steps in the catalytic oxidation and synthesis of hydrocarbons [141-142]. We study the reaction in detail to provide a deeper insight into the mechanistic aspects for the catalytic oxidation of methylidyne (CH) on a stepped Rh(211) surface, following a study on the planar Rh(111) surface. CH oxidation process on a stepped rhodium surface is important because steps offer adsorption and reaction sites at undercoordinated surface atoms [143]. Various theoretical and experimental findings suggest that reactants and products are more strongly bound at such sites resulting in concomitantly lower activation barrier to reaction [144-146]. Previous studies of CH on Rh(111) surface [147, 148], considered CH decomposition and subsequent oxidation of atomic carbon by oxygen. A recent study indicates that there is an alternative pathway for the catalytic oxidation of methylidyne on Rh(111) surface [149]. The fundamental question which still remains open is if defects such as steps alter the minimum energy pathway. We therefore carried out an analogous study on Rh(211) surface. The calculated equilibrium structures of the initial and final states as well as the transition state structures of the oxidation of methylidyne are shown in **Figure 5.4** as energy diagram.

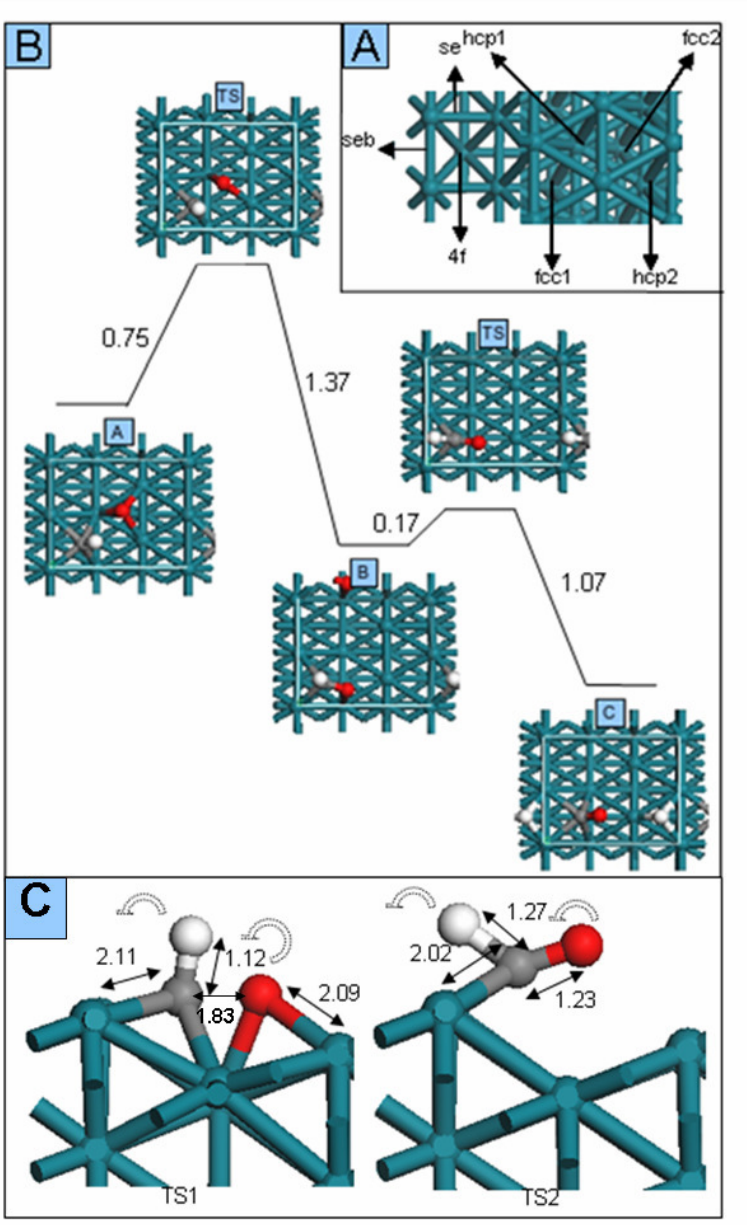


**Figure 5.4.** Panel A: Adsorption sites of Rh{211}. Labeled 4f is fourfold hollow, seb is step edge bridged, se is step bridged. Panel B: Energy diagram for surface oxidation of CH species (Reactant A) to CHO (Product B) via transition state (TS) and decomposition of CHO to CO and H (Product C) via TS. The activation energies are given in eV. Panel C: Transition state (TS) geometries. Hollow arrows indicate the direction of movement of atoms after TS.

CH adsorbing at a step edge is found more stable than on the terrace. The most stable adsorption site for CH is the four fold hollow site 4f. Dissociation of CH to atomic carbon and hydrogen is unlikely from 4f due to a rather high dissociation barrier of 1.04 eV and after dissociation the products could additionally undergo subsurface penetration, as indicated by calculations on (1 x 2) elementary cell. The next most stable site for CH adsorption is fcc1 and hcp1 site. We find that the activation barrier for CH dissociation from fcc1 is 0.61 eV, and from hcp1 is 1.07 eV. However, the diffusion barrier of CH from hcp1 to 4f is 0.65 eV and surprisingly the barrier from fcc1 to 4f is merely 0.05 eV. This low barrier will trigger fast diffusion of CH from the fcc1 to the 4f position and will consequently hinder the CH dissociation from fcc1 position. $CH_{(4f)}$ is the more stable species and this site will therefore be more populated and hence there will be a dynamic interplay of reaction and diffusion processes. Oxidation of CH by atomic oxygen leading to an oxomethylidyne (CHO) species is activated by 0.75 eV. The reaction is also found to be thermochemically favorable with energy of reaction of -0.62 eV. It should be mentioned that the CHO species has been inferred experimentally as a combustion intermediate on Pt(110) [46].

The CHO species formed by oxidation is bound to the surface via the carbon and oxygen atom and this species can subsequently undergo decomposition to adsorbed CO and H and the barrier of this reaction is found to be merely 0.17 eV, which is considerably lower than that of direct dissociation of CH. The reaction is exothermic (-0.90 eV) and so the reaction is kinetically as well as thermodynamically more favorable than decomposition of CH according to our DFT results. Our DFT results strongly suggests that CH diffuses to the 4f position very rapidly rather than to dissociate from the fcc1 position and hence we assume that the oxidation of $CH_{(4f)}$ is the main pathway for oxidation via CHO species. At a step the dissociation barrier is merely 50 % of the barrier on Rh(111). The two main reasons for this is that (i) the step is able to bind the transition state geometry more strongly than a flat surface, hence lowering the barrier and

(ii) the atoms at the step are under coordinated which also enhance the stabilization of the transition state, which also lowers the barriers.

## 5.3 Pathways and Activation Barriers for Reactions of $C_2H_x$ and Oxygen

Ethylidyne ($CH_3C$) is the most stable $C_2H_x$ species on Rh(111) surface obtained from ethane or propane dehydrogenation reactions. Experiments using variable temperature STM have indicated that ethane upon annealing from 160 K to 350 K give $CH_3C$ as a stable surface species also on Pt(111) [152]. $CH_3C$ surface intermediate is thus one of the most abundant species observed on ethane and ethylene dehydrogenation over close-packed fcc(111) and hcp(0001) metal surfaces [153-159]. Ethylidyne species is generated rapidly by decomposition of $CH_3CH$ species, which are formed upon alkane ($C_2$, $C_3$ etc.) decomposition.

Since $CH_3C$ is observed experimentally in surface, which is often detected from the reactions of ethane and ethylene on transition metal surfaces, it is intriguing to find out if can be activated by a co-adsorbed oxygen. We investigated the reaction of stable $CH_3C$ with oxygen, which is possibly one of the crucial elementary step for ethane catalytic partial oxidation. The interaction of oxygen with Rh(111) is however studied extensively experimentally [159 and references therein] as well as theoretically [161, 162 and references therein]. The activation energy for diffusion of $CH_3C$ from the hcp-hollow site to fcc-hollow site is 0.52 eV whereas it is 0.48 eV while starting from the fcc-hollow position. So, $CH_3C$ remains moderately mobile on Rh(111) at the temperatures relevant to the reaction.

Hydrogen abstraction from $CH_3C$ by a coadsorbed oxygen is unlikely due to high lying H atoms of the methyl group present in $CH_3C$ and the molecule has to undergo huge strain to bend completely in the transition state. We also obtained

from our DFT calculations very high barrier for the direct H abstraction and hence this step is ruled out.

Direct Reaction of ethylidyne with oxygen is studied in detail and found to be interesting in the way that a surface acetyl intermediate species $CH_3CO$ is formed on direct reaction. This reaction has activation energy of 1.48 eV and is exothermic with energy of reaction as -0.21 eV.

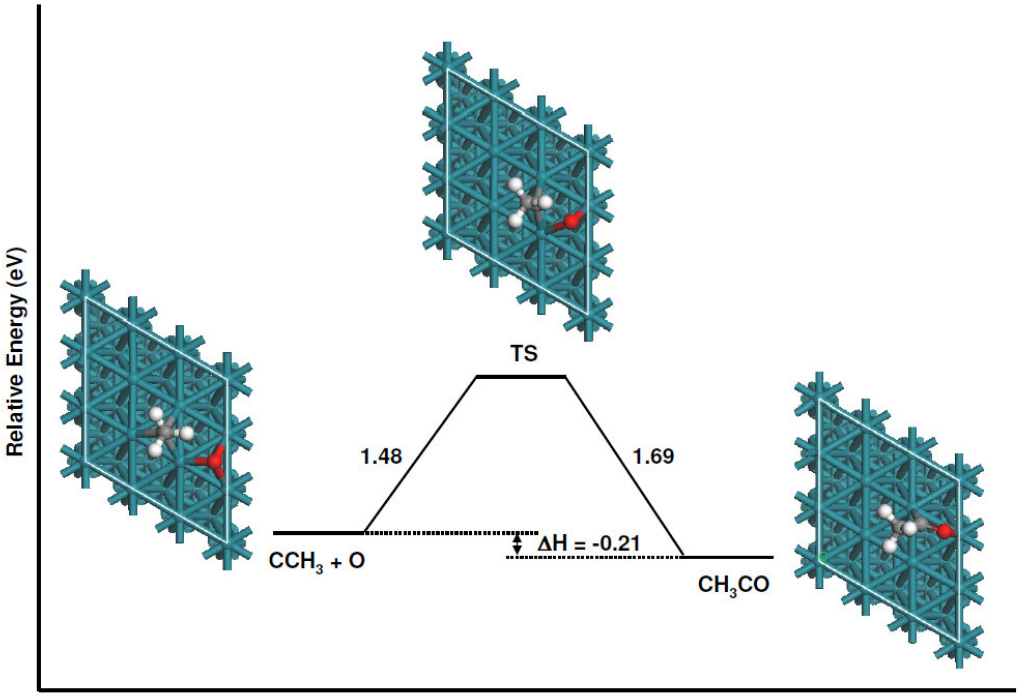


**Fig 5.5** Energy diagram for the reaction of oxygen with ethylidyne forming a surface aldehyde species and structures of initial, transition, and final state from left to right)

The activation energy thus obtained for direct reaction of $CH_3C$ with co-adsorbed O atom to form $CH_3CO$, is significantly lower than direct decomposition of $CH_3C$ to $CH_3$ and C by 0.62 eV. Another competing reaction in this case is dehydrogenation of $CH_3C$ to $CH_2C$ and H, but the reaction is found to be highly activated with activation energy 2.30 eV and is also endothermic by 0.33 eV. So among the competing reactions, $CH_3C$ will be more driven towards

oxidation in the surface in the presence of oxygen to form a surface aldehyde species and this particular reaction will prevail due to its comparatively low barrier and exothermicity.

Oxidation of ethylidyne takes place from its stable configuration at a hcp site and oxygen is also present in the neighboring hcp site when the $CH_3C$ is driven towards a bridged site and O atom also migrates to the nearby bridged site to form $CH_3CO$ with coordinating to the surface via C and O atom.

It is interesting to observe that $CH_3CO$ has been also studied for its attachment to BNNT nanotubes and has the similar structural orientations [163]. In can be noted that the acetyl intermediate has been detected experimentally using HREELS measurement over Pt(111) surface [164] .

The structural details of $CH_3CO$ are given below in Table 5.1. The molecule is attached to the surface in a bridged site via the C and O atoms bonding to the neighboring Rh atoms.

| $CH_3CO$ | | | | | | | | | |
|---|---|---|---|---|---|---|---|---|---|
| Dist. (Å) | **$Rh_1$-C** | **$Rh_2$-O** | **C-O** | **C-C** | **$H_1$-C** | **$H_2$-C** | **$H_3$-C** | **Rhc-Rh** | **Rhc-Rh** |
| | 1.98 | 2.18 | 1.26 | 1.50 | 1.10 | 1.10 | 1.10 | 0.23 | 0.17 |
| Angle (deg) | **$H_1$-C-C** | | **$H_2$-C-C** | | **$H_3$-C-C** | | **O-C-C** | **$Rh_1$-C-O** | **$Rh_2$-C-O** |
| | 110.83 | | 107.55 | | 111.45 | | 119.30 | 117.15 | 101.14 |

**Table 5.1** The geometrical parameters of $CH_3CO$

$CH_3CO$ obtained can undergo direct decomposition at C-C bond to form $CH_3$ and CO or it can be dehydrogenated to form $CH_2CO$ and H. According to our DFT calculations, we have found that the dehydrogenation reaction is dominant at this stage.

**Figure 5.6** and **Figure 5.7** represents the energy diagram for decomposition and dehydrogenation of $CH_3CO$ respectively.

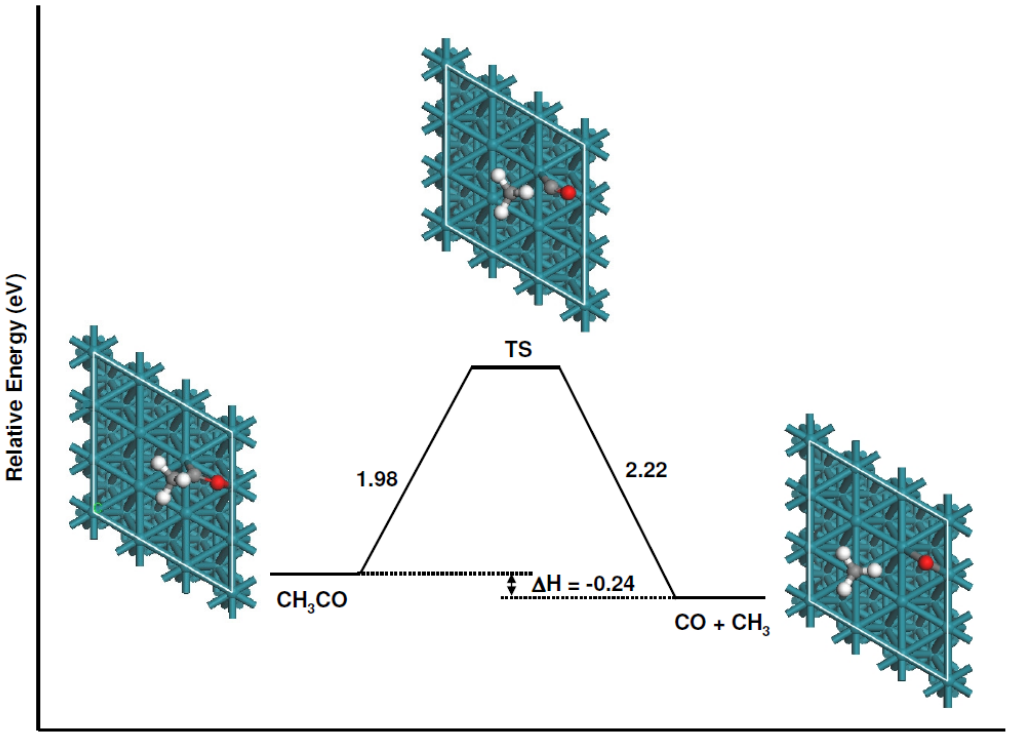


**Fig 5.6** Energy diagram for decomposition of $CH_3CO$ to $CH_3$ and CO

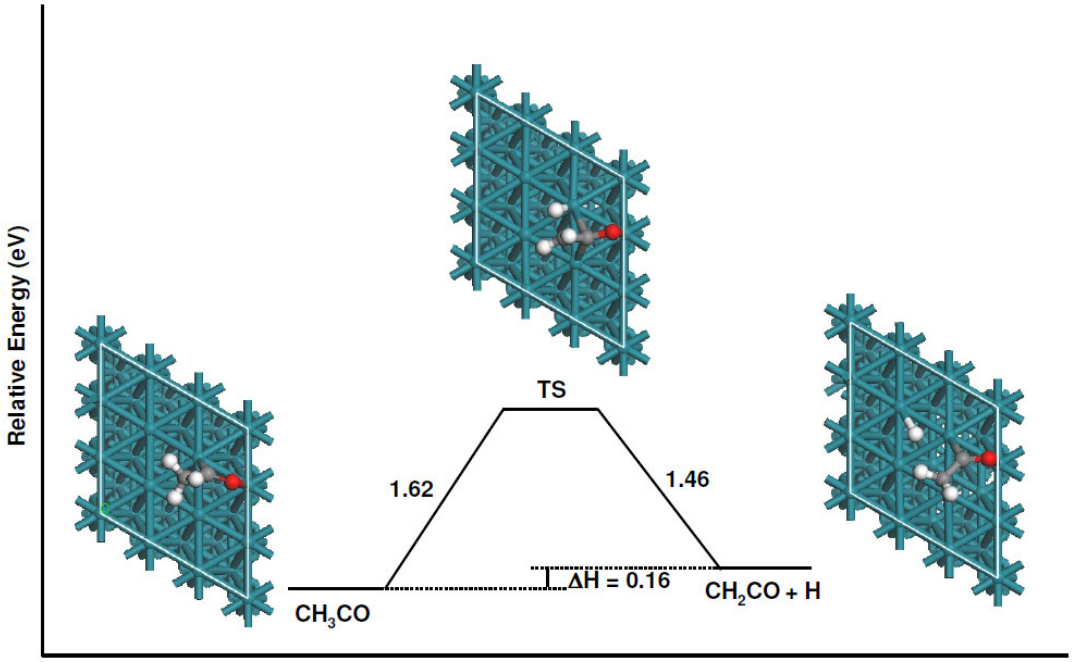


**Fig 5.7** Energy diagram for dehydrogenation of $CH_3CO$ to $CH_2CO$ and H

The $CH_2CO$ species formed at the Rh(111) surface remain coordinated to the surface via C and O atom like $CH_3CO$, however for $CH_2CO$, the C-C bond is shorter and closer to the surface.

| $CH_2CO$ | | | | | | | | | | |
|---|---|---|---|---|---|---|---|---|---|---|
| Distance (Å) | **$Rh_1$-$C_1$** | **$Rh_2$-$C_1$** | **$Rh_3$-$C_1$** | **$C_1$- $C_2$** | **$C_1$-O** | **$H_1$-$C_2$** | **$H_2$-$C_2$** | **$Rhc_1$-Rh** | **$Rhc_2$-Rh** | **Rho-Rh** |
| | 2.28 | 2.06 | 2.50 | 1.43 | 2.13 | 1.09 | 1.09 | 0.28 | 0.17 | 0.02 |
| Angle (deg) | **$H_1$-C-C** | | **$H_2$-C-C** | | **O-C-C** | | **$Rh_1$-C-O** | | **$Rh_2$-C-O** | |
| | 118.48 | | 116.93 | | 124.34 | | 116.97 | | 90.42 | |

**Table 5.2.** The geometrical parameters of $CH_2CO$

After the adsorption of $CH_2CO$, the surface reconstruction occurs and the neighboring surface Rh atoms are lifted by 0.17 to 0.28 Å. The geometrical parameters of the $CH_2CO$ are given in the **Table 5.2**. The $CH_2CO$ can further undergo dehydrogenation to form CHCO and H or decomposition via C-C bond breakage to form $CH_2$ and CO. $CH_2CO$ is oriented in such a way that C-C bond is much nearer to the surface as compared to $CH_3CO$ and hence C-C bond breakage occurs at this stage. During decomposition reaction, transition state consists of CO and $CH_2$ where CO occupies a bridged site and $CH_2$ migrates over a top Rh atom. The two C atoms fall apart by 2.17 Å in the TS. The fragmentation of $CH_2CO$ has the barrier of 1.49 eV and the energy of reaction is -0.34 eV.

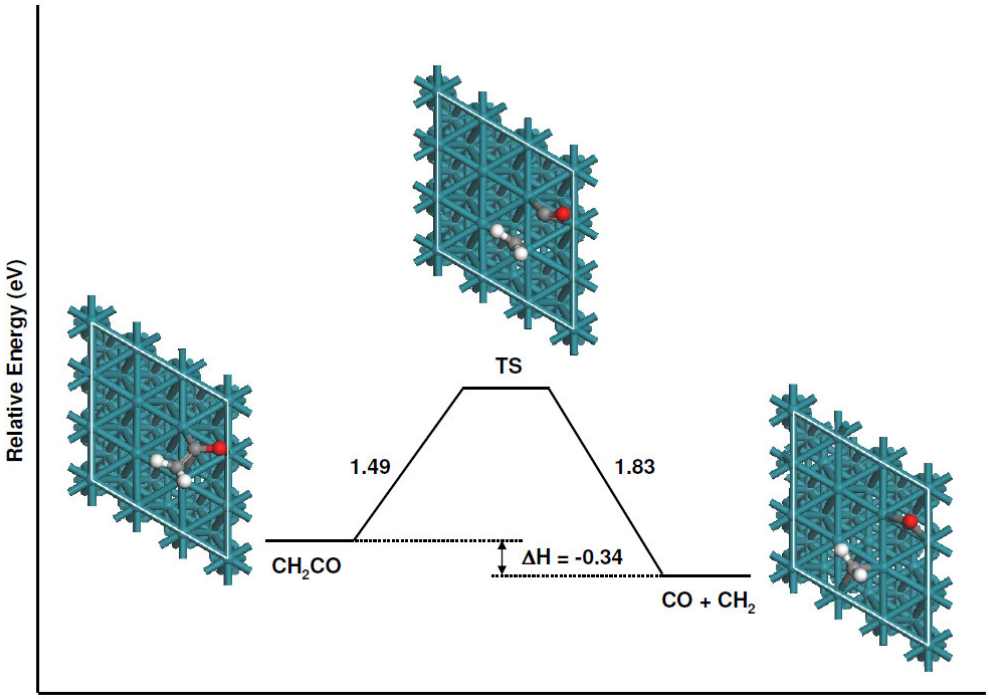


**Fig 5.8** Energy diagram for decomposition of $CH_2CO$ to $CH_2$ and CO

C-C bond dissociation in this case is more favorable energetically than C-H from $CH_2CO$ leading to the formation of adsorbed CO and $CH_2$. So, we obtain a alternative minimum energy pathway for the reaction of ethylidyne via $CH_3CO$ and $CH_2CO$, when a co-adsorbed oxygen atom is present in the system.

## 5.4 Conclusions

The important $CH_x$ (x=1-4) and $C_2H_x$ (x= 1-5) species, which are activated in the presence of oxygen are studied in the presence of coadsorbed oxygen. On of our basic investigation leads to the elucidation of lowest energy pathway for the reaction of methylidyne (CH) on Rh surface, which is one of the rate determining step for the activation of methane of noble metal surfaces. The oxidation of methylidyne (CH) via oxomethylidyne is found to be an exothermic process and is observed most likely at lower temperature, i.e., during the light-off of the catalysts. We establish that CPOx of CH on stepped Rh(211) surface is

energetically more favorable than the same on Rh(111) surface, owing to the lower activation barrier on the stepped surface. This study therefore confirms previous results on low-index surfaces and marks the first example of the low-energy oxomethylidyne pathway on a stepped surface. It moreover strongly suggests that alternative reaction pathways have to be considered in kinetic modelling of hydrocarbons in order to describe accurately the conversions especially during the light-off.

As we see in the chapter 4, that it is likely, $C_3H_x$ (x=2-7) fragments break into $C_2H_x$ (x=1-5) fragments on Rh(111) surface so it is likely that oxygen plays a role when there are $C_2$ and $C_1$ fragments are present in the surface due to their size and less steric hindrance that will occur with smaller molecules. We thus address some important reactions that will take place in the presence of oxygen. It is identified that methylidyne and ethylidyne are most susceptible to the reaction with co-adsorbed O as they form a stable species with O and this reactions are found to have the lowest energy pathway amongst competing reactions for both the species. These reactions are thus identified as dominating during catalytic partial oxidation.

# Chapter 6

# Conclusions and Outlook

In this thesis, we performed a systematic study of the adsorption of saturated hydrocarbons and their dissociation on metal surfaces. We used plane wave DFT method and periodic slab models for our study. Understanding the adsorbate-surface interaction and characterization of the surface structures and adsorption modes along with the calculation of the relative stabilities, reaction energies and reaction barriers are key steps to understand surface phenomena.

Ethane and Propane dissociative adsorption on a Rh(111) surface is studied and it is observed that this step is one of the rate determining steps. All the $C_2H_x$ (x=0-5) and $C_3H_x$ (x=2-7) fragments are characterized and the relative stabilities of the species are obtained. We obtained the geometries and preferred adsorption site for all the fragments produced from $C_2$ and $C_3$ hydrocarbons on Rh surface. DFT calculations for enable us to characterize even weakly adsorbed and short-lived reaction intermediates which are otherwise extremely difficult to isolate and study by experiments. The adsorption energies are computed for each reaction intermediate, which is a key step in the study of mechanism consisting of the possible reaction pathways. Our results are in good agreement with the experimental data available. For ethane dehydrogenation and fragmentation, each elementary step is studied and corresponding kinetic parameters are derived. Isomerization reactions are also taken into consideration. Similar calculations are carried out propane dehydrogenation. Since not much data is available in literature, these studies are a valuable addition for understanding the hydrocarbon chemistry on transition metal surfaces.

Microkinetic simulation using these DFT results and comparison to experimental data will be valuable future steps to provide quantitative insights into the complex catalytic processes. Based on the experiments on flow reactors, and the automatic generation of reaction pathways supported by quantum mechanical calculations, it will be possible to develop a detailed reaction mechanism on the catalyst surface. With this reaction mechanism, the reactors can be quantitatively simulated under conditions which are of technical relevance and with this some indication will be obtained for the optimization of the overall process. The interaction between experiment, modelling and numerical simulation will lead to the complete understanding of the process of catalytically supported partial oxidation over noble metals.

# References


1. D. A. Hickman and L. D. Schmidt, Science, 1993, 259, 343.
2. R. Schwiedernoch, S. Tischer, C. Correa and O. Deutschmann, Chem. Eng. Sci., 2003, 58, 633.
3. A. T. Ashcroft, A. K. Cheetham, M. L. H. Green and P. D. F. Vermon, Nature, 1991, 352, 225.
4. R. Schwiedernoch, S. Tischer, H. R. Volpp and O. Deutschmann, Studies Surface Science and Catalysis: Natural Gas ConVersion VII; Elsevier: Amsterdam, 2004, 147, 511.
5. J.N. Armor, Appl. Cat al. A. Gen., 1999, 176, 159.
6. L. Ma and D. L. Trimm, Appl. Catal. A. Gen., 1996, 138, 265.
7. A. K. Avci, D. L. Trimm and Z. I. Önsan, Chem. Eng. J., 2002, 90, 77.
8. Z. X. Liu, Z. O. Mao, J. M. Xu, N. Hess-Mohr and V. M. Schmidt, Chinese J. Chem. Eng., 2006, 14, 259.
9. B.S. Cağlayan, A.K. Avci, Z. I. Önsan, A.E. Aksoylu, Appl. Catal. A. Gen., 2005 280, 181.
10. A.K. Avci, D.L. Trimm, A.E. Aksoylu and Z. I. Önsan, Appl. Catal. A. Gen., 2004, 258, 235.
11. N. Sheppard, C. De la Cruz, Adv. Catal., 1996, 41, 1.
12. B. Hammer and J.K. Norskov, Adv. Catal., 2000, 45, 71.
13. S. T. Ceyer, Annu. Rev. Phys. Chem, 1988, 39, 479.
14. C. R. Arumainayagam and R. J. Madix, Progr. Surf. Sci, 1991, 38, 1
15. C. T. Rettner and M. N. R. Ashford, Dynamics of Gas-Surface Interactions. London, R. Soc. Chem., 1991.
16. R. J. D Miller and J. C. Tully, Surface Reaction Dynamics, Chemical Physics, 1996, 205, 275.
17. R. J. Hamers, J. Phys. Chem., 1996, 100, 13103

18. A. Szabo and N. S. Ostlund, Modern Quantum Chemistry, McGraw-Hill, New York, (1989).
19. M. Born and J. R. Oppenheimer, Annalen der Physik, 1927, 84, 457.
20. R. G. Parr and W. Yang, Density functional theory of atoms and molecules, Oxford University Press, New York, (1989).
21. W. Kohn and L. J. Sham, Phys. Rev., 1965, 140, 1133.
22. P. Hohenberg and W. Kohn, Phys. Rev., 1964, 136, B864.
23. J. P. Perdew and Y. Wang, Phys. Rev. 1992, 45, 13244.
24. O. R. Inderwildi, Multiscale Modelling for Automotive Exhaust-Gas Aftertreatment - From the Quantum Chemistry to the Engineering Level, PhD Thesis, Heidelberg University, 2005.
25. V. Milman, V. Winkler, J. A. White, C. J. Pickard, M. C. Payne, E. V. Akhmatskaya and R. H. Nobes, Int. Quant. Chem., 2000, 77, 895: M. C. Payne, M. P. Teter, D. C. Allan, T. A. Arias and J. D. Joannopoulos, Rev. Mod. Phys., 1992, 64, 1045.
26. M. D. Segall, P. J. D. Lindan, M. J. Probert, C. J. Pickard, P. J. Hasnip, S. J. Clark and M. C. Payne, J. Phys.: Cond. Matt., 2002, 14, 2717.
27. J. S. Blakemore, Solid State Physics Cambrige University Press, Cambridge, 1985.
28. M. P. Teter, D. C. Allan, T. A. Arias, J. D. Joannopoulos and M. C. Payne, Rev. Mod. Phys., 1992, 64, 1045.
29. D. Vanderbilt, Phys. Rev. B, 1990. 41, 7892.
30. G. Kresse and D. Joubert, Phys. Rev. B, 1999, 59, 1758.
31. D. J. Chadi and M. L. Cohen, Phys. Rev. B, 1973, 8, 5747.
32. J. D. Pack and H. J. Monkhorst, Phys. Rev. B, 1977, 16, 1748.
33. H. J. Monkhorst and J. D. Pack, Phys. Rev. B, 1976, 13, 5188.
34. O. R. Inderwildi and S. J. Jenkins, Chem. Soc. Rev., 2008, 37, 2274.
35. A. S. Bodke, D. A. Olschki, L. D. Schmidt and E. Ranzi, Science, 1999, 285, 712.

36. J. R. Rostrup-Nielsen, Catal. Today, 2000, 63, 159.
37. M. Dry, Catal. Today, 2002, 71, 227.
38. G. A. Somorjai, Introduction to Surface Chemistry and Catalysis, Wiley: New York, 1994.
39. I. Horiuti and M. Polanyi, Trans. Faraday Soc., 1934, 30, 1164.
40. W. H. Weinberg, J. Vac. Sc. Tech. A, 1992, 10, 2271.
41. M. A. Chesters, P. Gardner, E. M. McCAsh, Surf. Sc., 1989, 209, 89.
42. C. R. Arumainayagam, G. R. Schoofs, M. C. McMaster and R. J. Madix, J. Phys. Chem., 1991, 95, 1041.
43. F. Solymosi, L. Bugyi, A. Oszko, Langmuir, 1996, 12, 4145.
44. C. De La Cruza and S. Norman, Phys. Chem. Chem. Phys., 1999, 1, 329.
45. R. Hoffmann, Solids and surfaces, VCH, New York, 1988.
46. E. Schustorovich and R.C. Baetzold, Science, 1985, 227, 876.
47. H. Steininger, H. Ibach and S. Lehwald, Surf. Sci., 1982, 17, 685.
48. T. E. Felter and W. H. Weinberg, Surf. Sci., 1981, 103, 265.
49. J. Stohr, F. Sette and A. L. Johnston, Phys. Rev. Lett., 1984, 53, 1684.
50. G. W. Watson, R. P. K. Wells, D. J. Willock and G. J. Hutchings, J. Phys. Chem. B, 2000, 104, 6439.
51. V. Pallassana, M. Neurock, V. S. Lusvardi, J. J. Lerou, D. D. Kragten and R. A. van Santen, J. Phys. Chem. B, 2002, 106, 1656.
52. R. J. Koestner, M. A. van Hove and G. A. Somorjai, Surf. Sci., 1982, 121, 321.
53. A. Wander, M. A. van Hove and G. A. Somorjai, Phys. Rev. Lett., 1991, 67, 626.
54. L. H. Dubois, D. G. Castner and G. A. Somorjai, J. Chem. Phys., 1980, 72, 5234.
55. R. Levis and N. Winograd, J. Am. Chem. Soc., 1987, 109, 6873.
56. G. A. Somorjai, A. M. Contreras, M. Montano and R. M. Rioux, PNAS 2006, 103, 10577.

57. U. Starke, A. Barbieri, N. Materer, M. A. van Hove and G. A. Somorjai, Surf. Sci., 1993, 286, 1.

58. G. A. Somorjai, M. A. van Hove and B. E. Bent, J. Phys. Chem., 1988, 92, 973.

59. J. A. Gates and L. L. Kesmodel, Surf. Sci., 1983, 124, 68.

60. D. Stacchiola, M. Kaltchev, G. Wu and W. T. Tysoe, Surf. Sci., 2000, 470, L32.

61. T. S. Marinova and K. L. Kostov, Surf. Sci., 1987, 181, 573.

62. M. M. Hills, J. E. Parmeter, C. B. Mullins and W. H. Weiberg, J. Am. Chem. Soc., 1986, 108, 3554.

63. I. Jungwirthova and L. L. Kesmodel, J. Phys. Chem. B, 2001, 105, 674.

64. W. J. J. Harris, V. Fiorin, C. T. Campbell and D. A. King, J. Phys. Chem. B, 2005, 109, 4069.

65. A. B. Antonova, N. E. Kolobova, P. V. Petrovsky, B. V. Lokshin and N. S. Obezyuk, J. Organomet. Chem., 1977, 137, 55.

66. H. Ogasawara, S. Ichihara, H. Okuyama, K. Domen and M. Kawai, J. Electron Spectrosc. Relat. Phenom., 2001, 114/116, 339.

67. H. E. Newell, M. R. S. McCoustra, M. A. Chesters, C. De La Cruz, J. Chem. Soc. Faraday Trans., 1998, 94, 3695.

68. T. V. W. Janssens and F. Zaera, J. Phys. Chem., 1996, 100, 14118.

69. F. Zaera, T. V. W. Janssens and H. Öfner, Surf. Sci., 1996, 368, 371.

70. F. Zaera and N. Bernstein, J. Am. Chem. Soc., 1994, 116, 4881.

71. F. Zaera, Langmuir, 1996, 12, 88.

72. F. Zaera and C. R. French, J. Am. Chem. Soc., 1999, 121, 2236.

73. C-H Hwang, C-W Lee, H. Kang and C. M. Kim, Surf. Sc., 2001, 490, 144

74. E. A. Carter and B. E. koel, Surf. Sci., 1990, 226, 339

75. D. A. Hickman and L. D. Schmidt, J. Catal. 1992, 136, 300.

76. K. H. Hofstad, J. H. B. J. Hoebink, A. Holmen and G. B. Marin, Catal. Today, 1998, 40, 157.

77. D. A. Hickman and L. D. Schmidt, Science, 1993, 259, 343.
78. C. R. H. de Smet, M. H. J. M. de Croon, R. J. Berger, G. B. Martin and J. C. Schouten, Appl. Catal., 1999, 187, 33.
79. Q. G. Yan, T. H. Wu, W. Z. Weng, H. Toghiani, R. K. Toghiani, H. L. Wan and C. U. Jr. Pittman, J. Catal., 2004, 226, 247.
80. P. M. Torniainen, X. Chu and L. D. Schmidt, J. Catal., 1994, 146, 1.
81. A. L. Guimaraes, L. C. Dieguez and M. Schmal, J. Phys. Chem. B, 2003, 107, 4311.
82. L. Ma, D. L. Trimm and C. Jiang, Appl. Catal. A, 1996, 138, 275.
83. S. Ayabe, H. Omoto, T. Utaka, R. Kikuchi, K. Sasaki, Y. Teraoka and K. Eguchi, Appl. Catal. A, 2003, 241, 261.
84. J. Jr. Barbier and D. Duprez, Appl. Catal. A, 1992, 85, 89.
85. S. Liu, L. Xu, S. Xie, Q. Wang and G. Xiong, Appl. Catal. A, 2001, 211, 145.
86. T. Maillet, J. Jr. Barbier and D. Duprez, Appl. Catal. B, 1996, 9, 251.
87. M. Huff, P. M. Torniainen and L. D. Schmidt, Catal. Today, 1994, 21, 113.
88. F. Zaera and D. Chrysostomou, Surf. Sci., 2000, 457, 89.
89. F. Zaera and D. Chrysostomou, Surf. Sci., 2000, 457, 71.
90. A. M. Gabelnick, A. T. Capitano, S. M. Kane, J. L. Gland, D. A. Fischer, J. Am. Chem. Soc., 2000, 122, 143.
91. A. M. Gabelnick, D. J. Burnett, J. L. Gland and D. A. Fischer, J. Phys. Chem. B, 2001, 105, 7748.
92. A. Cassuto, M. Mane, G. Tourillon, P. Parent and J. Jupille, Surf. Sci., 1993, 287–288, 460.
93. J. A. Horsley, J. Stöhr and R. J. Koestner, J. Chem. Phys., 1985, 83, 3146.
94. C. E. Anson, N. Sheppard, B. R. Bender and J. R. Norton, J. Am. Chem. Soc., 1999, 121, 529.
95. R. J. Koestner, J. C. Frost, P. C. Stair, M. A. van Hove and G. A. Somorjai, Surf. Sci., 1982, 116, 85.

96. B. E. Bent, C. M. Mate, J. E. Crowell, B. E. Koel and G. A. Somorjai, J. Phys. Chem., 1987, 91, 1493.

97. A. Valcárcel , J. M. Ricart, A. Clotet , F. Illas , A. Markovits, C. Minot, J. Catal., 2006, 241, 115.

98. W. H. Weinberg and Y.-K. Sun, Science, 1991, 253, 542.

99. D. Chrysostomou, C. French and F. Zaera, Catal. Lett., 2000, 69, 117.

100. L. R. Holtzmeier, L.F. Albright, Symposium (international) on Combustion, 1969, 12, 375

101. M. Salmeron and G. A . Somorjai, J. Phys. Chem., 1982, 86, 341

102. K. M. Ogle, J. R. Creighton, S. Akhtar and J. M. White, Surf. Sc., 1986, 169, 246.

103. B. E. Bent, C. M. Mate, J. E. Crowell, B. E. Koel and G. A. Somorjai, J. Phys. Chem., 1987, 91, 1493

104. J. W. Peck, D. I. Mahon and B. E. Koel, Surf. Sci., 1998, 410, 200.

105. C. W. J. Bol, C. M. Friend, J. Am. Chem. Soc., 1995, 117, 8053.

106. Q. Y. Yang, K. J. Maynard, A. D. Johnson and S. T. Ceyer, J. Chem. Phys., 1995, 102, 7734.

107. C. -M. Chiang and B. E. Bent, Surf. Sci., 1992, 279, 79.

108. J. -L. Lin and B.E. Bent, Chem. Phys. Lett., 1992, 194, 208.

109. Y.L. Chan, P. Chaung and T.J. Chuang, J. Vac. Sci. Technol. A, 1988, 16, 1023.

110. A.V. Teplyakov, B.E. Bent, J. Eng Jr. and J.G. Chen, Surf. Sci., 1998, 399, L342.

111. C. –T. Au, C. –F. Ng and M. –S. Liao, J. Catal., 1999, 185, 12

112. P.M. Holmbad, J. Wamback and I. Chorkendorff, J. Chem. Phys., 1999, 110, 2637.

113. A.V. Walker and D.A. King, Phys. Rev. Lett., 1999, 82, 5156.

114. F. J. Weaver, F. A. Carlson and, J. R. Madix, Surf. Sci. Rep., 2003, 50, 107.

115. A.T. Gee, B.E. Hayden and C. Mormiche, J. Chem. Phys., 2003, 118, 3334.

116. A.C. Luntz, J. Chem. Phys., 1995, 102, 8264.
117. M.N. Carre´ and B. Jackson, J. Chem. Phys., 1998, 108, 3722.
118. Y. Xiang and J.Z.H. Zhang, J. Chem. Phys., 2003, 118, 8954.
119. P. Kratzer, B. Hammer and J.K. Nørskov, J. Chem. Phys., 1996, 105, 5595.
120. A. Bukoski, D. Blumling and I. Harrison, J. Chem. Phys., 2003, 118, 843.
121. D.T.P. Watson, S. Titmuss and D.A. King, Surf. Sci., 2002, 505, 49.
122. M.A. Peterson, S.J. Jenkins and D.A. King, J. Phys. Chem. B, 2004, 108, 5909.
123. M.A. Peterson, S.J. Jenkins and D.A. King, J. Phys. Chem. B, 2004, 108, 5920.
124. M. Valden, N. Xiang, J. Pere and M. Pessa, Appl. Surf. Sci., 1996, 99, 83.
125. R. M. Watwe, B. E. Spiewak, R. D. Cortright and J. A. Dumesic, J. Catal., 1998, 180, 184.
126. J. Kua and W. A. Goddard, J. Phys. Chem. B, 1998, 102, 9492.
127. J. Kua and W. A. Goddard, J. Phys. Chem. B, 1999, 103, 2318.
128. G. Papoian, J. K. Norskov and R. Hoffmann, J. Am. Chem. Soc., 2000, 122, 4129.
129. C. Minot, M. A. van Hove and G. A. Somorjai, Surf. Sci., 1983, 127, 441.
130. A. Michaelides and P. Hu, The Valency Effect on Reaction Pathways in Heterogeneous Catalysis: Insight from Density Functional Theory Calculations. In Theoretical Aspects of Heterogeneous Catalysis; Nascimento, M., Ed.; Kluwer Academic Publishers: Dordrecht and Boston, 2001.
131. M. A. Petersen, S. J. Jenkins and D. A. King, J. Phys. Chem. B, 2004, 108, 5909.
132. B. S. Bunnik and G. J. Kramer, J. Catal., 2006, 242, 309.
133. O. R. Inderwildi and S. J. Jenkins, J. Am. Chem. Soc., 2007, 129, 1751.
134. C. Puglia, A. Nilsson, B. Hernnas, O. Karis, P. Bennich and N. Martensson, Surf. Sci., 1995, 342, 119-133.

135. M. P. Zum Mallen and L. D. Schmidt, J. Catal., 1996, 161, 230.
136. M. Chen, S. P. Bates, R. A. van Santen and C. M. Friend, J. Phys. Chem. B, 1997, 101, 10051.
137. C. W. J. Bol and C. M. Friend, J. Am. Chem. Soc., 1995, 117, 11572.
138. C. E. Smith, J. P. Biberian and G. A. Somorjai, J. Catal., 1979, 57, 426.
139. D. M. Newns, Phys. Rev., 1969, 178, 1123; P. W. Anderson, Phys. Rev. 1961, 124, 41.
140. K. C. Wong, W. Liu, K. A. R. Mitchell, Surf. Sci., 1996, 360, 137.
141. M. P. Andersson, F. Abild-Pedersen, I. N. Remediakis, T. Bligaard, G. Jones, J. Engbæk, O. Lytken, S. Horch, J. H. Nielsen, J. Sehested, J. Rostrup-Nielsen, J. K. Nørskov and I. Chorkendorff, J. Catal., 2008, 255, 6.
142. O. R. Inderwildi, S. J. Jenkins and D. A. King, Angew. Chem., 2008, 47, 1-4.
143. M. Mavrikakis, M. Baeumer, H. –J. Freund and J. K. Nørskov, Catalysis Letters, 2002, 81, 153.
144. J. J. C. Geerling, J. H. Wilson, G. J. Kramer, H. P. C. E. Kuipers, A. Hoek and H. M. Huisman, Appl. Catal. A., 1999, 186, 27.
145. J. Rostrup-Nielsen and J. K. Nørskov, Topics in Catalysis, 2006, 40, 45.
146. Z. Liu and P. Hu, J. Am. Chem. Soc., 2002, 125, 1958.
147. C. T. Au, M. S. Liao and C. F. Ng, Chem. Phys. Lett., 1997, 267, 44.
148. B. S. Bunnik and G. J. Kramer, J. Catal., 2006, 242, 309.
149. O. R. Inderwildi and S. J. Jenkins, J. Am. Chem. Soc., 2007, 129, 1751.
150. D. T. P. Watson, J. J. W. Harris and D. A. King, Surf. Sci., 2002, 505, 58.
151. T. A. Land, T. Michely, R. J. Behm, J. C. Hemminger and G. Comsa, J. Chem. Phys., 1992, 97, 6774.
152. A. T. Anghel, S. J. Jenkins, D. J. Wales and D. A. King, J. Phys.Chem. B, 2006, 110, 4147.
153. S. G. Podkolzin, R. Alcala and J. A. Dumesic, J. Mol. Catal. A: Chem., 2004, 218, 217.

154. P. S. Cremer, X. C. Su, Y. R. Shen and G. A. Somorjai, J. Am. Chem. Soc., 1996, 118, 2942.

155. S. Azad, M. Kaltchev, D. Stacchiola, G. Wu and W. T. Tysoe, J. Phys. Chem. B 2000, 104, 3107.

156. R. I. Masel, Principles of Adsorption and Reaction on Solid Surfaces; Wiley: New York, 1996.

157. P. M. Parlett and M. A. Chesters, Surf. Sci., 1996, 358, 791.

158. T. A. Land, T. Michely, R. J. Behm, J. C. Hemminger and G. Comsa, J. Chem. Phys., 1992, 97, 6774.

159. M. V. Ganduglia-Pirovano and M. Scheffler, Phys. ReV. B: Solid State, 1999, 59, 15533.

160. T. Bhattacharjee, O. R. Inderwildi, S. J. J. Jenkins, U. Riedel and J. Warnatz, J. Phys. Chem., 2008, 112, 8751.

161. O. R. Inderwildi, D. Lebiedz, O. Deutschmann and J. Warnatz, J. Chem. Phys., 2005, 122, 154702.

162. M. Chen, S. P. Bates, R. A. van Santen and C. M. Friend, J. Phys. Chem. B, 1997, 101, 10051.

163. H. Roohi, A. Nowroozi, A. Ebrahimi and B. Makiabadi, Journal of Molecular structure: THEOCHEM, 2010, 952, 36.

164. H. Zhao, J. Kim and B. E. Koel, Surf. Sc., 2003, 538, 147548.

# Abbreviations

| | |
|---|---|
| CPOx | Catalytic Partial Oxidation |
| DFT | Density Functional Theory |
| HREELS | High Resolution Electron Energy Loss Spectroscopy |
| IRRAS | Infra Red Reflection Absorption Spectroscopy |
| LEED | Low Energy Electron Diffraction |
| NEXAFS | Near-Edge X-ray Absorption Fine Structure |
| RAIRS | Reflection Adsorption Infrared Spectroscopy |
| SFG | Sum Frequency Generation |
| TOF-SIMS | Time-Of-Fly Secondary Ion Mass Spectroscopy |
| TDS | Thermal Desorption Spectroscopy |
| XPD | X-ray Photoelectron Diffraction |
| XPS | X-ray Photoelectron Spectroscopy |

# Acknowledgements

The work presented in this thesis has been carried out by me in the Interdisciplinary Centre for Scientific Computing (IWR), University of Heidelberg, Germany.

I am deeply indebted to late Prof. Dr. Dr. h. c. Jürgen Warnatz who gave me the opportunity to work at IWR. I am very much thankful to my research supervisor Prof. Dr. Olaf Deutschmann for the guidance and inspiration. I express my sincere thanks and gratitude to Prof. Dr. Uwe Riedel for the co-supervision and various administrative help during the entire course of my work in Heidelberg.

I also thank Dr. Oliver R. Inderwildi for helpful scientific discussions.

It is a pleasure to acknowledge the cooperation and encouragement I received during the work from my colleagues, friends and staff members in the IWR. I thank Mrs. Ingrid Helwig for administrative assistance.

I feel greatly enriched and motivated by the supportive role of my family members all throughout, in particular the incredible pleasuring role of my daughter Shrinita.

Finally I wish to acknowledge the financial assistance from the Deutsche Forschung Gemeinschaft (DFG), Deutschland.

# Erklärung

Hiermit versichere ich, dass ich die Arbeit selbständig verfasst und keine anderen als die angegebenen Quellen und Hilfsmittel verwendet habe.

Heidelberg, den 27.06.2011

Tanushree Bhattacharjee